Activation and *in vivo* evolution of the MAIT cell transcriptome in mice and humans reveals diverse functionality

Authors: Timothy SC Hinks[1,2]*, Emanuele Marchi[3], Maisha Jabeen[2], Moshe Olshansky[4], Ayako Kurioka[3], Troi J Pediongco[1], Bronwyn S Meehan[1], Lyudmila Kostenko[1], Stephen J Turner[4], Alexandra J Corbett[1], Zhenjun Chen[1], Paul Klenerman[5] and James McCluskey[1]

Affiliations

1. Department of Microbiology and Immunology, Peter Doherty Institute for Infection and Immunity, University of Melbourne, Parkville, Victoria 3000, Australia.

2. Respiratory Medicine Unit and National Institute for Health Research (NIHR) Oxford Biomedical Research Centre (BRC), Nuffield Department of Medicine Experimental Medicine, University of Oxford, OX3 9DU, Oxfordshire, UK

3. Peter Medawar Building for Pathogen Research and Translational Gastroenterology Unit, Nuffield Department of Clinical Medicine, University of Oxford, OX3 3SY

4. Infection and Immunity Program and The Department of Biochemistry and Molecular Biology, Biomedicine Discovery Institute, Monash University, Clayton, Australia.

Contact information:

* Corresponding author and lead contact: Dr TSC Hinks, Respiratory Medicine Unit, NDM Experimental Medicine, University of Oxford, Level 7, John Radcliffe Hospital, Oxford, OX3 9DU timothy.hinks@ndm.ox.ac.uk; +44 1865 220885 @HinksLab

Abstract

Mucosal-associated invariant T (MAIT) cells are MR1-restricted innate-like T cells conserved across mammalian species, including mice and humans. By sequencing RNA from sorted MR1-5-OP-RU tetramer^{+} cells derived from either human blood or murine lungs, we define the basic transcriptome of an activated MAIT cell in both species and demonstrate how this profile changes during resolution and reinfection phases of infection. We observe strong similarities between MAIT cells in humans and mice. Compared with previously published T cell transcriptomes, MAIT cells displayed most similarity to iNKT cells when activated, but to γδ T cells, after resolution of infection. In both species activation leads to strong expression of pro-inflammatory cytokines and chemokines, and also a strong tissue repair signature, recently described in murine commensal-specific H2-M3-restricted T cells. These data define the requirements for, and consequences of, MAIT cell activation, revealing a tissue repair phenotype expressed upon MAIT cell activation in both species.

Key words

Mucosal-associated invariant T cell, T cell, transcriptome, MHC-related protein 1, activation, lung, human, mouse, riboflavin.

Mucosal-associated invariant T (MAIT) cells are innate-like T cells which express a 'semi-invariant' αβ T cell receptor (TCR) and recognise metabolic derivatives of riboflavin biosynthesis[1-3] presented on the restriction molecule major histocompatibility complex (MHC)-related protein-1 (MR1)[4,5]. These antigens, which include the potent MAIT cell ligand 5-(2-oxopropylideneamino)-6-D-ribitylaminouracil (5-OP-RU)[6], are produced by a wide variety of bacteria, mycobacteria and yeasts[1,7], but are absent from mammals, and therefore allows host – pathogen discrimination. MAIT cells have a strong pro-inflammatory phenotype, and produce interferon-γ (IFN-γ), TNF and IL-17A after phorbol myristate acetate (PMA) and ionomycin stimulation[8].

Whilst baseline frequencies of MAIT cells are low in specific-pathogen free C57BL/6 mice, we, and others, have previously shown that MAIT cells can be activated and expand *in vivo* in response to pulmonary infection with specific intracellular bacteria expressing the riboflavin pathway – *Salmonella* Typhimurium[9], *Legionella spp*[10], and *Francisella tularensis*[11,12] – or in response to synthetic 5-OP-RU accompanied by a Toll-like receptor agonst[9], providing valuable models to dissect MAIT cell biology.

To date the requirements for TCR-dependent activation of MAIT cells *in vivo* have not been systematically characterised, nor have the consequences of such activation been fully defined. Here we have used MR1 tetramers[2] loaded with 5-OP-RU to specifically identify MAIT cells from human peripheral blood and murine lungs, allowing us to assess the requirements for, and consequences of, MAIT cell activation *ex vivo* and *in vivo*. Using a transcriptomic approach on sorted MR1-5-OP-RU tetramer$^+$ cells we define the transcriptome of an activated MAIT cell in both species and explore how this changes during the resolution and reinfection phases of infection.

Our data reveal strong similarities between MAIT cells in humans and in mice at a transcriptional level, show that MAIT cells displayed the closest similarities to invariant natural killer T (iNKT) cells when activated, but after resolution of infection were more comparable to γδ T cells, and reveal a previously unknown tissue repair phenotype expressed upon MAIT cell activation in both species.

Results

Activation requirements of MAIT cells *in vivo*

First we aimed to test, systematically, the activation requirements of MAIT cells *in vivo* in mouse lungs. We have previously shown that pulmonary MAIT cell frequencies in mice can be markedly enhanced by intranasal administration of 5-OP-RU if it is co-administered with S-[2,3-bis(palmitoyloxy)propyl] cysteine (Pam2Cys), CpG ODN 1668 or polyinosinic:polycytidylic acid (poly I:C), which are agonists for TLR2/6, TLR9 and TLR3, respectively. We therefore investigated agonists for each of the murine TLRs, using the maximum doses presented in a literature review of previous studies of these compounds. All animals received the relevant TLR intranasally on day 0. In experimental animals this was administered in combination with 76 pmol 5-OP-RU on day 0, with repeated inoculae of 76 pmol 5-OP-RU on days 1, 2 and 4. Control mice received the same TLR ligand and 76 pmol of the non-activating MR1 ligand 6-formyl pterin (6-FP) according to the same schedule, or the TLR ligand alone (Supplementary Table S1). We observed 15-180-fold enrichment of pulmonary $CD3^{+}CD45.2^{+}CD19^{-}$MR1-5-OP-RU $tetramer^{+}$ MAIT cell frequencies at day 7, after administration of 5-OP-RU with agonists

of TLR3 (high molecular weight poly I:C), TLR4 (Lipopolysaccharide from *E.coli*), TLR2/6 (FSL-1 (Pam2CGDPKHPKSF)) and TLR9 (CpG ODN1826), but not with agonists of TLR1/2 (Pam3CSK4), TLR2 (heat killed *Listeria monocytogenes*), TLR5 (Flagellin from *S.typhimurium*), TLR7 (Imiquimod)(Figure 1), suggesting there is a specific and restricted range of danger signals that are capable of providing the necessary co-stimulus to drive MAIT cell accumulation in response to 5-OP-RU antigen.

Transcriptomic profile of activated human and murine MAIT cells

Having explored the requirements for activation of MAIT cells, we sought to describe in detail the consequences of their activation using a transcriptomic approach to define the basic transcriptome of a MAIT cell in both humans and mice and to determine how this is modulated by activation. Fresh human peripheral blood cells were obtained from three donors. These were cultured for 6 hours with ('stimulated') or without ('unstimulated') 10 nM 5-OP-RU, magnetically enriched on MR1-tetramer$^+$ cells, and flow-sorted for RNA sequencing of live CD3$^+$TCR Vα7.2$^+$ MR1-5-OP-RU tetramer+ MAIT cells, and of unstimulated naïve live CD8$^+$CD45RA$^+$ T cells as a comparator cell type **(Table 1).**

We have previously shown that pulmonary infection of mice with the intracellular pathogen *Legionella longbeachae* induces strong TCR-mediated MAIT cell activation, and that this plays a significant role in host immune protection, thus constituting a physiologically relevant model of *in vivo* MAIT cell activation. Using this model, which induces a rapid and sustained expansion of MAIT cells in the lung (Supplementary figure S1) we therefore included within the same sequencing experiment live pulmonary CD3$^+$45.2$^+$19$^-$MR1-5-OP-RU tetramer$^+$ MAIT cells which were magnetically enriched and

109 flow-sorted from the lungs of mice 7 days after infection with $1x10^4$ CFU *L. longbeachae*
110 ('acute'), or at least 12 weeks post infection ('resolution') or 7 days after a second
111 intranasal infection with $2x10^4$ CFU *L. longbeachae* in mice that had recovered from
112 infection 12 weeks previously ('reinfection'). Live $CD3^+CD45.2^+CD19^-CD8^+CD44^-$
113 $CD62L^+$ naïve T cells from uninfected mice were used as a comparator cell type.

114 The number of differentially expressed genes (DEG) in activated MAIT cells
115 compared with naïve $CD8^+$ T cells was 4613 genes in human 5-OP-RU-stimulated MAIT
116 cells, and 3758 genes in acutely infected mice at a false discovery rate (FDR) p value of
117 <0.05 and minimum $\log_{(2)}$ fold change of ±1 (Numbers of DEG are shown in Table 2; full
118 lists of DEG are shown in Supplementary tables S2 and S3). These genes constitute the
119 basic transcriptome of an activated MAIT cell in each species. To explore the nature of
120 these gene profiles further we compared different activation states of MAIT cells. In
121 humans 3227 genes were differentially expressed between stimulated and unstimulated
122 MAIT cells and could therefore be considered the direct signature of TCR-mediated MAIT
123 cell activation, whilst 968 genes were differentially expressed between unstimulated MAIT
124 cells and naïve $CD8^+$ T cells, and therefore are more related to constitutive differences
125 between T cell lineages (Supplementary table S2). In mice 1889 genes were differentially
126 expressed between acute infection and resolution of infection, analogous to the signature
127 of TCR-mediated activation (Supplementary table S3).

128 Analysis of TCR genes over-represented in MAIT cells confirmed highly
129 significant selective use of TRAV1-2 with TRBV6-4, TRBV6-1 and TRBV20-1 in humans
130 and Trbv13-5 with Trav1 and Traj33 in mice, in MAIT cells compared naïve CD8 T cells,
131 as expected[4,5,13,14] (Supplementary tables S4, S5).

Focussed analysis of known cytokine genes confirmed a strong upregulation of several pro-inflammatory type 1 and type 17 cytokines, especially CSF2 (GM-CSF), IL-17A, LIF, TNF, IFN-γ, and IL-17F) which were highly upregulated in both mouse and human in activated MAIT cells (Tables 3,4). Expression of selected cytokines was confirmed by flow cytometry (Supplementary figures S2, S3). Likewise there was significant, but more modest, upregulation of LTA (lymphotoxin A) and CSF1 (M-CSF) in both species. Some features were observed only in one species, notably IL-2 and TNSF14 (LIGHT) produced by activated human MAIT cells, and Tnfsf11 (TRANCE, RANKL) by murine MAIT cells. In contrast to activation-induced cytokines, expression of the anti-apoptotic cytokine IL-15, implicated in the development and maturation of memory $CD8^+$ T cells[15], was restricted to MAIT cells in their resting state: human unstimulated MAIT cells, or murine MAIT cells at resolution of infection. In mice resolution of infection was also associated specifically with strong expression of Tnfsf18 (GITRL), confirmed by flow cytometry. Expression of cytokine receptors is shown in Supplementary tables S6, S7 and of recognised 'CD markers' in Supplementary tables S8, S9.

Similar analysis of chemokines showed strong activation-induced upregulation of a range of chemokines, including XCL1, CCL3 (MIP1α), CCL4 (MIP1β), and CXCL16 common to both species (Supplementary tables S10, S11), and of a common array of chemokine receptors CCR6, CXCR6, CCR1, CCR2 and CCR5 (Supplementary tables S12,S13, Supplementary figure S2), underlining marked evolutionary conservation of MAIT cell function.

Pathway analysis of the MAIT cell transcriptome

To analyse the transcriptome at the level of pathways, rather than individual genes, we looked for upregulation of pathways using the open source, manually curated, peer-reviewed Reactome database[16]. The main pathways upregulated in human 5-OP-RU stimulated MAIT cells compared with naïve $CD8^+CD45RA^+$ T cells were related to endoplasmic reticulum stress – the unfolded protein response, and the related pathways IRE-1-α activation of chaperones and XBP1(S) activation of chaperones – to chemokine receptor-ligation, and to cholesterol biosynthesis (Figure 2A). When stimulated human MAIT cells were contrasted directly with unstimulated MAIT cells the activation of chemokine and cytokine signalling pathways – chemokine receptor-ligation, IL-2 signalling, interleukin receptor SHC signalling – was more apparent, as was human solute carrier-mediated transmembrane transport (Figure 2B).

Perhaps reflective of the different context of activation, and consistent with the very rapid MAIT cell expansion observed with infection *in vivo*[10], the murine MAIT cells activated by acute *L. longbeachae* infection showed very strong activation of cell cycle pathways as well as signalling by RHO GTPases and chemokine receptor-ligation, with similar dominance of the cell cycle when MAIT cells activated by acute infection were contrasted directly with unstimulated MAIT cells after infection resolution (Figure 2C,D).

Comparison of MAIT cell transcriptomic profile with other T cell subsets

MAIT cells are a relatively ancient T cell subset, with both innate and adaptive properties, and are capable of expressing diverse functions depending on the nature of the pathogenic encounter[10,17]. Therefore we sought next to explore the nature of the murine MAIT cell transcriptome by comparing it with the transcriptional profiles for a wide range of other

177 cell types reported within the Immunological Genome Project database[18]. Using
178 hierarchical clustering, whilst the pulmonary naïve $CD8^{+}CD44^{-}CD62^{+}$ T cells clustered
179 with reference naïve $CD8^{+}$ splenic T cells, activated MAIT cells from acute primary
180 infection or from acute reinfection clustered most closely to invariant NKT cells (Figure
181 3). By contrast, after resolution of the infection MAIT cells clustered most closely with
182 unstimulated splenic γδ T cells.

183 **MAIT cells express a tissue repair transcriptional profile**

184 Our observation of a distinct cytokine signature after infection resolution
185 suggested that MAIT cells might be capable of performing more diverse functions than a
186 purely pro-inflammatory response to TCR ligation. As observed already, TCR ligation in
187 the absence of a TLR-agonist did not induce proliferation of murine MAIT cells. A wide
188 variety of bacteria, mycobacteria and yeasts, including many commensal organisms[19]
189 express the riboflavin biosynthetic pathway, and may therefore be a major source of
190 activating MR1 ligands, constitutively, or during breach of a barrier surface. Indeed MAIT
191 cells require commensal organisms for their expansion[20]. A class of skin-homing Tc17
192 cells specific to commensal flora has recently been described, which expresses a 'tissue
193 repair' gene signature and can accelerate repair of an epithelial wound[21]. These cells share
194 several features with non-classical T cells, including the Type-17 cytokine profile and
195 restriction by another MHC class 1b antigen presentation molecule H2-M3. Therefore we
196 asked whether this tissue repair phenotype was a shared transcriptional programme in
197 MAIT cells. We used gene set enrichment analysis[22] (GSEA) to compare expression of this
198 set of tissue repair genes[21] (Supplementary table S14) with genes differentially expressed
199 in MAIT cells. Indeed this gene set was markedly enriched in human MAIT cells after 5-

OP-RU stimulation (normalised enrichment score (NES) 1.38, family-wise error rate (FWER) P<0.01, Figure 4A, B, Table 5). Similarly, despite differences in species, timecourse and method of MAIT cell activation, the same gene set was even more highly enriched in mice during acute *L. longbeachae* infection (NES 1.38, FWER P<0.01, Figure 4C, D, Table 5), with enrichment of ten genes common to both analyses (TNF, CSF2, HIF1A, FURIN, VEGFB, PTGES2, PDGFB, TGFB1, MMP25).

Discussion

Here we have systematically investigated the requirements for TCR-mediated activation of MAIT cells in mice, and delineated both *ex vivo* in human and *in vivo* in mice the consequences of this activation at a transcriptomic level. Due to their pro-inflammatory cytokine profile[8] and specificity for a restricted selection of microbially-derived small molecules[2,23], the most immediately apparent function of MAIT cells has hitherto been the early detection of microbes and initiation of an inflammatory host response[7,11,12,24,25]. Consistent with previous studies, our data confirm MAIT cells' capacity for a strong, rapid pro-inflammatory response. However, in contrast to the similarities between activated MAIT cells and iNKT cells, the close similarity at a transcriptional level of resting murine MAIT cells to γδ T cells and the discovery of a clear transcriptional signature for tissue repair suggests that MAIT cells potentially have much broader roles in mucosal immunity.

The nature of these roles may depend on the context and nature of the cells' activation. As with iNKT cells[26] MAIT cells may be activated either via TCR recognition of ligand presented on MR1, or via cytokines alone, in the absence of a TCR signal, as occurs during respiratory viral infection[17,27,28]. As we have observed previously, in the absence of inflammatory cytokines TCR-ligation alone is not sufficient to produce MAIT

cell proliferation and activation *in vivo*[9]. Rather a second signal is required. *In vitro* in humans it has been shown that agonists of TLR1, TLR2, and TLR6 can provide this co-stimulus to drive MAIT cell cytokine secretion[29]. Consistent with, and extending these previous observations[9], we observed here that murine MAIT cells proliferated in response to a different, but similarly restricted, set of TLR agonists: those for TLR3, TLR4, TLR6/2 and TLR9 and, but not for other TLRs tested.

As MAIT cells are found at their highest frequencies in the lungs and liver[11,30,31] and the MR1-axis is highly conserved[5] – implying a strong evolutionary pressure – it could be expected that potent MAIT cell responses should be elicited by a range of major human pathogens, and yet to date a strong human clinical phenotype for MAIT cell deficiency has not been described, and even in animal models the protective effect afforded by MAIT cells against mortality has been relatively modest in fully immune competent hosts[10,11], likely due to multiple layers of immunological redundancy provided by other arms of innate and adaptive immunity[10]. One explanation might be that a different, more subtle function of MAIT cells explains Nature's ongoing requirement for this subset in effective mucosal immunity.

Our data suggest an entirely novel function for MAIT cells in tissue repair. In both human and murine datasets, activated MAIT cells highly express a shared a gene expression signature with murine H2-M3 restricted commensal-specific Tc17 cells recently reported by Linehan *et al*[21]. Using topical skin colonisation with a specific clade of *S. epidermidis* this group demonstrated that specific commensal-derived *N*-formylated peptides presented on H2-M3, another class 1b MHC molecule, could induce tissue-resident Tc17 cells which provided specific capacity to promote tissue repair and

246 remodelling (MMP25, Furin, PDGFB, TGFB1) and angiogenesis (CSF2, VEGFA,
247 PDGFB)[21]. Healing of skin wounds was shown to be accelerated by colonisation of H2-
248 M3 sufficient mice with these commensals. A human equivalent of H2-M3 has yet to be
249 identified, but MAIT cells are abundant at barrier sites, allowing close interactions with
250 commensal bacteria possessing an intact riboflavin metabolic pathway. Similarly to H2-
251 M3 restricted $CD8^+$ T cells, in this position MAIT cells are poised to maintain tissue
252 homeostasis in the presence of commensals thereby limiting inflammation and associated
253 tissue injury[32]. These data are consistent with a similar finding of this same tissue repair
254 signature observed by GSEA analysis of MAIT cells when activated by TCR triggering,
255 but not observed in the context of cytokine-mediated activation[33]. These findings might
256 also explain the increased gut permeability observed in *Mr1*$^{-/-}$ NOD mice compared with
257 *Mr1*$^{+/-}$ NOD littermates, which suggested a protective role for MAIT cells for maintaining
258 gut homeostasis[34]. It was been speculated this might be mediated by IL-17A and IL-22[34]
259 which are both important in intestinal homeostasis[35,36], and in the case of IL-22 induction
260 of protective mucus-producing goblet cells[37]. In our dataset both cytokines were strongly
261 upregulated in activated murine MAIT cells. Thus during mucosal damage, riboflavin-
262 synthesising pathogens and commensal organisms might provide the MAIT cell activation
263 both to induce the necessary inflammatory response to ensure bacterial clearance and also
264 the signals necessary to accelerate healing of the wound. After successful clearance of
265 infection, or barrier repair, the subsequent reduction in MR1-Ag presentation would ensure
266 this signal declined.

267 Commensals might drive the MR1-MAIT cell axis in other ways. MAIT cell
268 expansion requires exposure to a commensal microbiome[20]. Furthermore, commensal

269 microbes have been implicated in enhancing host immunity against pathogens in the
270 respiratory tract. In mice a Nod2-mediated IL-17A response to upper respiratory tract
271 commensals enhanced CSF2 (GM-CSF) to promote bacterial killing and clearance by
272 alveolar macrophages[38]. The strong upregulation of CSF2 (GM-CSF) we observed
273 following TCR stimulation in human and murine MAIT cells would be beneficial in
274 clearance of pathogenic microorganisms which have crossed the mucosal barrier. During
275 tissue homeostasis commensal-derived MR1 signals might drive lower level, constitutive
276 expression of GM-CSF needed to maintain alveolar macrophages in a pathogen responsive
277 state[38].

278 Another novel, prominent feature of MAIT cell activation in both humans and mice
279 was the marked expression of the IL-6 family cytokine leukaemia inhibitory factor (LIF).
280 Consistent with our finding of a MAIT cell tissue-repair signature, LIF has been found to
281 be protective against epithelial damage in murine models of pneumonia[39]. LIF is
282 significantly induced during pneumonia and can reduce lung epithelial cell death,
283 promoting the expression of tissue-protective genes essential to lung regeneration and
284 repair, and increased mucosal barrier integrity.

285 A unique feature of our transcriptomic dataset is that in a single experiment we
286 were able to analyse MAIT cells from two different species obtained from two different
287 tissues, using different contexts of activation, and yet we observed that the transcriptomic
288 profiles of these MAIT cells were in fact very similar. Thus the distinctive, common
289 properties of MAIT cells predominate over differences between these cells which might be
290 observed in different contexts. Again, this underlines a strong conservation of functions
291 likely driven by a consistent role in mucosal immunology.

Given the wide diversity of conventional and non-classical T cells now recognised[24], many of which share common transcriptional programmes[40,41] we applied a comparative approach[42] to analyse the phenotype of MAIT cells, overcoming significant methodological hurdles to compare our RNA sequencing data directly with older microarray expression data in the ImmGen dataset. Activated MAIT cells were most similar to activated invariant iNKT cells, as might be expected from the similarities in surface markers and functional phenotype[5,24,43]. This is likely related to shared transcriptional signatures controlled by common transcription factors, not least that which has been described for promyelocytic leukemia zinc finger (PLZF) which defines a distinct surface phenotype and functional capacity in $CD161^{+}$ NK cells, iNKT cells and MAIT cells[40]. However it is interesting that in their resting state MAIT cells more closely resembled splenic γδ T cells. Unlike MAIT and iNKT cells, most γδ T cells are not constrained by a specific MHC restriction[44,45], rather they have different functional profiles associated with usage of different TCR V gene segments. Depending on the Vγ subset, γδ T cells recognise a diverse range of small microbial metabolites, lipids, self-antigens and stress-induced proteins, and may display a range of functions associated with variously with inflammation, immunoregulation, cytotoxicity, antigen presentation[24] and promotion of tissue repair[46]. In the absence of the TCR/TLR mediated activation, MAIT cells may be fulfilling a different, perhaps homeostatic function. Indeed, we were able to investigate what this might be by analysing the transcriptome of MAIT cells in their resting state, outside the context of inflammation. After resolution of infection, Tnfsf18 (Glucocorticoid-Induced TNF-Related Ligand, GITRL) is the most strongly upregulated cytokine. The function of GITRL is context dependent, but under resting, non-inflammatory it can

315 negatively regulate NK cells and maintain or expand regulatory T cells conditions[47]. Other
316 immunoregulatory cytokines were also upregulated: Tnfsf11 (TRANCE, RANKL) was
317 identified in a commensal-derived immunoregulatory signature[21], whilst IL-15 can inhibit
318 T cell apoptosis to maintain memory T cell survival[48]. Together these data implicate resting
319 MAIT cells in potentially significant immunoregulatory roles.

320 In summary, our analysis of TCR-activated MAIT cells demonstrates pronounced
321 conservation of functions and gene expression profiles between human and murine cells,
322 and suggests that beyond type 17 / type 1 pro-inflammatory responses to invading
323 microbial pathogens, MAIT cells have the capacity to contribute to immunoregulatory and
324 tissue repair roles likely to be essential for maintaining the integrity of mucosal barrier
325 surfaces in health and disease.

326

327 **Materials and Methods**

328 Animal models

329 C57BL/6 mice were bred and housed in the Biological Research Facility of the Peter
330 Doherty Institute (Melbourne, Victoria, Australia). Mice aged 6–12 weeks were used in
331 experiments, after approval by the University of Melbourne Animal Ethics Committee
332 (1513661 and 1513712).

333 Intranasal (i.n.) inoculation with a stimulatory MR1 ligand (76 pmol 5-OP-RU) or
334 a non-activating MR1 ligand (76 pmol 6-FP) and TLR agonist (see Table S1) in a total 50
335 µl volume was performed on isofluorane-anaesthetised mice on day 0. Additional doses of
336 the relevant MR1 ligand in 50 µl were administered on days 1, 2, and 4. Control mice
337 received TLR agonists alone, in a total volume of 50 µl. For infection experiments mice

were inoculated with 1-2 x10^4 CFU *Legionella longbeachae* (clinical isolate NSW150) in 50 µl PBS.

Mice were weighed daily and assessed visually for signs of disease, including inactivity, ruffled fur, laboured breathing, and huddling behaviour. Animals that had lost ≥15% of their original body weight and/or displayed evidence of pneumonia were euthanised.

Mice were killed by CO_2 asphyxia, the heart perfused with 10 ml cold Roswell Park Memorial Media-1640 (RPMI, Gibco) and lungs were taken. To prepare single-cell suspensions lungs were finely chopped with a scalpel blade and treated with 3 mg.ml^{-1} collagenase III (Worthington, Lakewood, NJ), 5 µg/ml DNAse, and 2% foetal calf serum in RPMI for 90 min at 37°C with gentle shaking, and, where relevant, brefeldin A (GolgiPlug™, BD Biosciences, San Diego, CA). Lung cells were then filtered (70 µm) and washed with PBS/2% foetal calf serum. Red blood cells were lysed with hypotonic buffer TAC (Tris-based amino chloride) for 5 min at 37°C. Approximately 1.5x10^6 cells were filtered (40 µm) and used for flow cytometric analysis. To obtain sufficient cells for sorting naïve $CD8^+CD44^-CD62L^+$ cells from infection-naïve mice lungs from 2-3 mice per sample were pooled and stained with 0.18 µl anti-CD8-PE, then magnetically enriched using anti-PE beads (Miltenyi) prior to sorting.

For analysis of systemic MAIT cell distribution lymphocytes were obtained from mesenteric lymph nodes by passing through a 70 µm strainer. Splenocytes were obtained by homogenising splenic tissue through a 70 µm strainer then preforming red cell lysis prior to staining. Peripheral blood cells were obtained from the inferior vena cava into a heparinised syringe and underwent surface staining prior to red cell lysis with 1 ml of 10%

361 red cell lysis buffer (BD Bioscience) for 5 minutes at room temperature before washing
362 twice with FACS buffer. Hepatic lymphocytes were obtained by perfusing the liver with
363 8-10 ml PBS, passing through a 40 μm strainer, washing once with PBS the resuspending
364 in 36% Percoll (Sigma) and centrifuging without braking at 800 *g* for 25 mins at RT over
365 a 70% Percoll underlay. Cells from the interphase were washed with FACS buffer, red cells
366 lysed with 1 ml 10% red cell lysis buffer, cells washed twice and stained for flow
367 cytometry.
368
369 Determination of bacterial counts in infected lungs
370 Bacterial infection was determined for *L. longbeachae* by counting colony-forming units
371 (CFU) obtained from plating homogenised lungs in duplicate from infected mice (x5 per
372 group) on buffered charcoal yeast extract agar (BYCE) containing 30 μg/ml streptomycin
373 and colonies counted after 4 days at 37°C under aerobic conditions. Culture media for other
374 bacteria are shown in table S2.
375
376 Antibodies flow cytometry and cell sorting
377 Details of flow cytometry antibodies are shown in Supplementary table S15. To block non-
378 specific staining, cells were incubated with MR1-6-FP tetramer and anti-Fc receptor
379 (2.4G2) for 15 min at room temperature and then incubated at room temperature with
380 Ab/tetramer cocktails in PBS/2% foetal calf serum. Dead cells were excluded using 4′,6-
381 diamidino-2-phenylindole (DAPI) for live cell sorting added for 10 mins or by staining for
382 20 mins in PBS with fixable viability dyes Zombie Yellow (Biolegend, 1:100, 423104) or
383 Live/Dead EF780 (BD Bioscience, 1:1000, 565388).

For live cell sorting on human peripheral blood mononuclear cells (PBMC) 50ml of heparinised blood were obtained freshly per volunteer, mixed with an equal volume of phosphate buffered saline (PBS) and layered over an equal volume of Ficoll-Paque (GE Healthcare, Chicago, IL) and centrifuged at 800 *g* for 20 mins at room temperature. Cells were washed twice with PBS, cells counted by trypan blue estimation, then half the cells were resuspended overnight in RPMI with 10% human serum for overnight rest and the other half resuspended in flow cytometry buffer comprising PBS with 2% foetal calf serum and 2 mM EDTA (FACS buffer) for immediate magnetic enrichment and sorting. These cells were stained with surface antibodies (CD3-PE-CF594, CD8-PerCPCy5.5, CD45RA-FITC, TCR Vα7.2-APC and FCγ block for 15 mins at RT, followed by staining with MR1-5-OP-RU tetramer-PE for 20 mins at RT. Tetramer positive cells were positively selected using anti-PE microbeads (10 μl per 10^{-7} cells, Miltenyi, Cologne, Germany) according to the manufacturer's instructions. Cells were sorted immediately into ice cold PBS with 10% FCS using an FACSAria III cell sorter (BD Bioscience) selecting live $CD3^{+}$TCR-$V\alpha7.2^{+}$MR1-5OP-RU-$tetramer^{+}$ MAIT cells from the positive fraction and live $CD3^{+}CD8^{+}CD45RA^{+}$MR1-$Tetramer^{-}$ cells from the negative fraction. The following day the remaining cells were stimulated for 6 h with 10 nM 5-OP-RU then magnetically enriched using MR1-5-OP-RU-tetramer-PE and anti-PE microbeads, and live $CD3^{+}$TCR-$V\alpha7.2^{+}$MR1-5-OP-RU-$tetramer^{+}$ MAIT cells sorted in the same manner. Purity was checked and with an average of 98%. Immediately after sorting cells were centrifuged at 400 *g* for 5 mins then resuspended in 100 μL of RNA lysis buffer (Agilent Ltd, UK) with 0.7 μL β-mercaptoethanol and stored at -80ºC.

For live cell sorting of murine T cells, CD8 cells were magnetically enriched using anti-CD8-PE and anti-PE microbeads and live $CD8^+CD44^-CD62L^+$ cells from uninfected mice, or live $CD3^+CD19^-CD45.2^+TCR\beta^+$MR1-5-OP-RU-tetramer$^+$ MAIT cells from previously infected mice were sorted as above.

For intracellular staining, cells were fixed with 1% paraformaldehyde prior to analysis on LSRII or LSR Fortessa or Canto II (BD Biosciences) flow cytometers. For intracellular cytokine staining Golgi plug (BD Biosciences) was used during all processing steps. Cells stimulated with PMA (phorbol 12-myristate 13-acetate;)/ionomycin (20 ng ml^{-1}, 1μg ml^{-1}, respectively) for 3 h at 37°C were included as positive controls. Surface staining was performed at 37°C, and cells were stained for intracellular cytokines using the BD Fixation/Permeabilization Kit (BD, Franklin Lakes, NJ) or transcription factors using the transcription buffer staining set (eBioscience) according to the manufacturers' instructions.

For validation of key targets identified by RNA sequencing flow cytometry was performed on cryopreserved human PBMC from additional healthy human donors. Samples were defrosted into pre-warmed RPMI with 10% human serum, stained with anti-TCR-Vα7.2-PE or anti-TCR-Vα7.2-PE and magnetically enriched using anti-PE or anti-APC microbeads. 200,000 positively-selected TCR-$V\alpha7.2^+$ cells or the negative fraction (for naïve $CD8^+45RA^+$ cells) were co-cultured for 5 hours in the presence of brefeldin A with 100,000 class I reduced (C1R) antigen presenting cells (APCs) which had been previously pulsed for 2 hours with 10 nM 5-OP-RU, or with naïve C1R cells (unstimulated control), or with PMA / ionomycin (20 ng ml^{-1}, 1μg ml^{-1}, respectively), or without any stimulation. Cells were then analysed by surface and intracellular cytokine staining as

429 above. For validation of murine targets cells were isolated from uninfected mice or mice
430 which had undergone intranasal infection 7 days prior (acute) or 12 weeks prior (resolution)
431 or reinfection 7 days prior, and cytometrically analysed as described above.
432
433 RNA sequencing
434 Cells were lysed in Agilent lysis buffer (Agilent Ltd., UK) containing 100 mM β-
435 mercaptoethanol and passed through a QIAshredder device (Qiagen, Valencia, US),
436 then RNA extracted using the Absolutely RNA Nanoprep Kit according to the
437 manufacturer's instructions, including using of DNase I. RNA libraries were prepared at
438 the Melbourne Translational Genomics Platform, Department of Pathology (The
439 University of Melbourne). Briefly, RNA quality and quantity were assessed using the
440 Bioanalyzer 2100 RNA pico kit (Agilent technologies). The input total RNA was
441 normalized to 250 pg per sample and median RIN was 9.7 (range 5.7-10.0). RNA was
442 reverse transcribed and cDNA amplified by *in vitro* transcription with the SMART-Seq v4
443 Ultra Low Input RNA Kit for Sequencing (Clontech). First strand cDNA synthesis and
444 tailing by reverse transcription was performed using Clontech's proprietary SMART
445 (Switching Mechanism at 5' End of RNA Template) technology. Following first strand
446 synthesis, cDNA was amplified 12 cycles by LD PCR using blocked PCR primers.
447 Amplified cDNA was purified using AMPure XP prior to QC using the bioanalyser 2100
448 HS DNA kit (Agilent technologies). Library preparation of purified amplified cDNA was
449 performed using Nextera XT library preparation (Illumina, AUS). Following QC, 150 pg
450 of cDNA was tagmented (simultaneously fragmented with adaptors inserted) using Nextera
451 transposons. Molecular barcodes were incorporated during 12 cycles of amplification

452 followed by purification using AMPure XP. The libraries passed a quality checkpoint
453 (Qubit and Bioanalyser HS DNA) prior to normalization and pooling before loading onto
454 the HiSeq 2500 (Illumina, AUS) for paired end sequencing.
455
456 Quality control and bioinformatics analysis of RNA sequencing data
457 RNA-seq reads were aligned to reference genome sequences using STAR[49] aligner
458 software. Mapped reads were assigned to genomic features using *Rsubread*[50] R package[51].
459 Genes that were differentially expressed (>2 fold, P<0.01, FDR<0.05) between
460 conditions and their normalised expression values, were generated with *EdgeR* R
461 package[52], Partek® Flow®, an online analysis platform for Next Generation Sequencing
462 data (http://www.partek.com/partek-flow/). Pathway enrichment analysis using the
463 Reactome platform[16] was performed using *ReactomePA*[53] R package. Gene count data
464 transform to log2-counts per million (logCPM) was performed using *voom* function in
465 *limma*[54] R package. Gene set enrichment analysis (GSEA) using *voom* transformed count
466 data was performed using GSEA version 3.0[55], comparing gene expression data as a whole
467 with the reference gene list obtained from the publication by Linehan et al.[21]
468 RNA-seq data (logCPM) and ImmGen microarray data were integrated using a
469 common set of *Entrez*[56] annotated genes; batch effect removal was performed using
470 *ComBat* algorithm in *sva*[57] R package. Hierarchical clustering analysis of transcription
471 profiles was conducted in R employing highly variable genes (IQR >0.75[58]) and Euclidian
472 distance.
473
474 Standard statistical analysis
475 Statistical tests were performed using the Prism GraphPad software (version 7.0 La Jolla,
476 CA). Comparisons between groups were performed using Student's t-tests or Mann-
477 Whitney tests as appropriate unless otherwise stated. Flow cytometric data analysis was
478 performed with FlowJo10 software (Ashland, OR).

Reagents

Human peripheral blood mononuclear cells (PBMC) were obtained from the Australian Red Cross Blood Service (ARCBS) (University of Melbourne Human Research Ethics Committee 1239046.2). Healthy human lung explant tissue was obtained via the Alfred Lung Biobank program and ARCBS from organs not suitable for donation (Blood Service HREC 2014#14 and University of Melbourne Human Research Ethics Committee 1545566.1).

Compounds, immunogens and tetramers

5-OP-RU was prepared as described previously[6]. CpG1668 (Sequence: T*C*C*A*T*G*A*C*G*T*T*C*C*T*G*A*T*G*C*T (*phosphorothioate linkage) nonmethylated cytosine-guanosine oligonucleotides was purchased from Geneworks (Thebarton, Australia) and Pam2Cys was chemically synthesised and functionally verified in house. Other toll like receptor ligands are detailed in Supplementary table S1. Murine and human MR1 and β2-Microglobulin genes were expressed in *Escherichia coli* inclusion bodies, refolded, and purified as described previously[59]. MR1-5-OP-RU tetramers were generated as described previously[2].

Bacterial strains

Cultures of *Legionella longbeachae* NSW150 were grown at 37°C in buffered yeast extract (BYE) broth supplemented with 30-50 μg/ml streptomycin for 16 hours to log-phase (OD600 0.2-0.6) with shaking at 180 rpm. For the infecting inoculum, bacteria were re-

inoculated in pre-warmed medium for a further 2–4 h culture (OD_{600} 0.2–0.6) with the estimation that 1 OD_{600}=5x10^8/ml, sufficient bacteria were washed and diluted in phosphate buffered saline (PBS) with 2% BYE for i.n. delivery to mice. A sample of inoculum was plated onto (BYCE) with streptomycin for verification of bacterial concentration by counting colony-forming units.

References:

1. Kjer-Nielsen, L., *et al.* MR1 presents microbial vitamin B metabolites to MAIT cells. *Nature* **491**, 717-723 (2012).
2. Corbett, A.J., *et al.* T-cell activation by transitory neo-antigens derived from distinct microbial pathways. *Nature* **509**, 361-365 (2014).
3. Eckle, S.B., *et al.* Recognition of Vitamin B Precursors and Byproducts by Mucosal Associated Invariant T Cells. *J Biol Chem* **290**, 30204-30211 (2015).
4. Tilloy, F., *et al.* An invariant T cell receptor alpha chain defines a novel TAP-independent major histocompatibility complex class Ib-restricted alpha/beta T cell subpopulation in mammals. *J Exp Med* **189**, 1907-1921 (1999).
5. Porcelli, S., Yockey, C.E., Brenner, M.B. & Balk, S.P. Analysis of T cell antigen receptor (TCR) expression by human peripheral blood CD4-8- alpha/beta T cells demonstrates preferential use of several V beta genes and an invariant TCR alpha chain. *J Exp Med* **178**, 1-16 (1993).
6. Mak, J.Y., *et al.* Stabilizing short-lived Schiff base derivatives of 5-aminouracils that activate mucosal-associated invariant T cells. *Nature communications* **8**, 14599 (2017).
7. Le Bourhis, L., *et al.* Antimicrobial activity of mucosal-associated invariant T cells. *Nat Immunol* **11**, 701-708 (2010).
8. Dusseaux, M., *et al.* Human MAIT cells are xenobiotic-resistant, tissue-targeted, CD161hi IL-17-secreting T cells. *Blood* **117**, 1250-1259 (2011).
9. Chen, Z., *et al.* Mucosal-associated invariant T-cell activation and accumulation after in vivo infection depends on microbial riboflavin synthesis and co-stimulatory signals. *Mucosal immunology* **10**, 58-68 (2017).
10. Wang, H., *et al.* MAIT cells protect against pulmonary Legionella longbeachae infection. *Nature communications* **9**, 3350 (2018).
11. Meierovics, A., Yankelevich, W.J. & Cowley, S.C. MAIT cells are critical for optimal mucosal immune responses during in vivo pulmonary bacterial infection. *Proc Natl Acad Sci U S A* **110**, E3119-3128 (2013).
12. Meierovics, A.I. & Cowley, S.C. MAIT cells promote inflammatory monocyte differentiation into dendritic cells during pulmonary intracellular infection. *J Exp Med* **213**, 2793-2809 (2016).
13. Reantragoon, R., *et al.* Antigen-loaded MR1 tetramers define T cell receptor heterogeneity in mucosal-associated invariant T cells. *J Exp Med* **210**, 2305-2320 (2013).
14. Lepore, M., *et al.* Parallel T-cell cloning and deep sequencing of human MAIT cells reveal stable oligoclonal TCRbeta repertoire. *Nature communications* **5**, 3866 (2014).
15. Jabri, B. & Abadie, V. IL-15 functions as a danger signal to regulate tissue-resident T cells and tissue destruction. *Nat Rev Immunol* **15**, 771-783 (2015).
16. Fabregat, A., *et al.* The Reactome Pathway Knowledgebase. *Nucleic acids research* **46**, D649-D655 (2018).
17. van Wilgenburg, B., *et al.* MAIT cells contribute to protection against lethal influenza infection *in vivo*. *Nature communications* **9**(2018).

18. Heng, T.S., Painter, M.W. & Immunological Genome Project, C. The Immunological Genome Project: networks of gene expression in immune cells. *Nat Immunol* **9**, 1091-1094 (2008).
19. Kanehisa, M. & Goto, S. KEGG: Kyoto encyclopedia of genes and genomes. *Nucleic acids research* **28**, 27-30 (2000).
20. Treiner, E.*, et al.* Selection of evolutionarily conserved mucosal-associated invariant T cells by MR1. *Nature* **422**, 164-169 (2003).
21. Linehan, J.L.*, et al.* Non-classical Immunity Controls Microbiota Impact on Skin Immunity and Tissue Repair. *Cell* **172**, 784-796 e718 (2018).
22. Mootha, V.K.*, et al.* PGC-1alpha-responsive genes involved in oxidative phosphorylation are coordinately downregulated in human diabetes. *Nat Genet* **34**, 267-273 (2003).
23. Kjer-Nielsen, L.*, et al.* MR1 presents microbial vitamin B metabolites to MAIT cells. *Nature* **491**, 717-723 (2012).
24. Godfrey, D.I., Uldrich, A.P., McCluskey, J., Rossjohn, J. & Moody, D.B. The burgeoning family of unconventional T cells. *Nat Immunol* **16**, 1114-1123 (2015).
25. Le Bourhis, L.*, et al.* MAIT Cells Detect and Efficiently Lyse Bacterially-Infected Epithelial Cells. *PLoS Pathog* **9**, e1003681 (2013).
26. Holzapfel, K.L., Tyznik, A.J., Kronenberg, M. & Hogquist, K.A. Antigen-dependent versus -independent activation of invariant NKT cells during infection. *J Immunol* **192**, 5490-5498 (2014).
27. van Wilgenburg, B.*, et al.* MAIT cells are activated during human viral infections. *Nature communications* **7**, 11653 (2016).
28. Loh, L.*, et al.* Human mucosal-associated invariant T cells contribute to antiviral influenza immunity via IL-18-dependent activation. *Proc Natl Acad Sci U S A* **113**, 10133-10138 (2016).
29. Ussher, J.E.*, et al.* TLR signalling in human antigen-presenting cells regulates MR1-dependent activation of MAIT cells. *Eur J Immunol* **46**, 1600-1614 (2016).
30. Rahimpour, A.*, et al.* Identification of phenotypically and functionally heterogeneous mouse mucosal-associated invariant T cells using MR1 tetramers. *J Exp Med* **212**, 1095-1108 (2015).
31. Greene, J.M.*, et al.* MR1-restricted mucosal-associated invariant T (MAIT) cells respond to mycobacterial vaccination and infection in nonhuman primates. *Mucosal immunology* **10**, 802-813 (2017).
32. Klenerman, P. & Ogg, G. Killer T cells show their kinder side. *Nature* **555**, 594-595 (2018).
33. Leng, T.*, et al.* TCR and inflammatory signals tune human MAIT cells to exert specific tissue repair and effector functions. *bioRxiv* (2018).
34. Rouxel, O.*, et al.* Cytotoxic and regulatory roles of mucosal-associated invariant T cells in type 1 diabetes. *Nat Immunol* **18**, 1321-1331 (2017).
35. Lee, J.S.*, et al.* Interleukin-23-Independent IL-17 Production Regulates Intestinal Epithelial Permeability. *Immunity* **43**, 727-738 (2015).
36. Dudakov, J.A., Hanash, A.M. & van den Brink, M.R. Interleukin-22: immunobiology and pathology. *Annu Rev Immunol* **33**, 747-785 (2015).
37. Sugimoto, K.*, et al.* IL-22 ameliorates intestinal inflammation in a mouse model of ulcerative colitis. *J Clin Invest* **118**, 534-544 (2008).

38. Brown, R.L., Sequeira, R.P. & Clarke, T.B. The microbiota protects against respiratory infection via GM-CSF signaling. *Nature communications* **8**, 1512 (2017).
39. Quinton, L.J.*, et al.* Leukemia inhibitory factor signaling is required for lung protection during pneumonia. *J Immunol* **188**, 6300-6308 (2012).
40. Kurioka, A.*, et al.* CD161 Defines a Functionally Distinct Subset of Pro-Inflammatory Natural Killer Cells. *Frontiers in immunology* **9**, 486 (2018).
41. Cohen, N.R.*, et al.* Shared and distinct transcriptional programs underlie the hybrid nature of iNKT cells. *Nat Immunol* **14**, 90-99 (2013).
42. Lee, Y.J.*, et al.* Lineage-Specific Effector Signatures of Invariant NKT Cells Are Shared amongst gammadelta T, Innate Lymphoid, and Th Cells. *J Immunol* **197**, 1460-1470 (2016).
43. Eckle, S.B.*, et al.* A molecular basis underpinning the T cell receptor heterogeneity of mucosal-associated invariant T cells. *J Exp Med* **211**, 1585-1600 (2014).
44. Chien, Y.H., Meyer, C. & Bonneville, M. gammadelta T cells: first line of defense and beyond. *Annu Rev Immunol* **32**, 121-155 (2014).
45. Vantourout, P. & Hayday, A. Six-of-the-best: unique contributions of gammadelta T cells to immunology. *Nat Rev Immunol* **13**, 88-100 (2013).
46. Havran, W.L. & Jameson, J.M. Epidermal T cells and wound healing. *J Immunol* **184**, 5423-5428 (2010).
47. Clouthier, D.L. & Watts, T.H. Cell-specific and context-dependent effects of GITR in cancer, autoimmunity, and infection. *Cytokine & growth factor reviews* **25**, 91-106 (2014).
48. Malamut, G.*, et al.* IL-15 triggers an antiapoptotic pathway in human intraepithelial lymphocytes that is a potential new target in celiac disease-associated inflammation and lymphomagenesis. *J Clin Invest* **120**, 2131-2143 (2010).
49. Dobin, A.*, et al.* STAR: ultrafast universal RNA-seq aligner. *Bioinformatics* **29**, 15-21 (2013).
50. Liao, Y., Smyth, G.K. & Shi, W. The Subread aligner: fast, accurate and scalable read mapping by seed-and-vote. *Nucleic acids research* **41**, e108 (2013).
51. Team, R.C. R: A language and environment for statistical computing. . (R Foundation for Statistical Computing, Vienna, Austria, 2014).
52. Robinson, M.D., McCarthy, D.J. & Smyth, G.K. edgeR: a Bioconductor package for differential expression analysis of digital gene expression data. *Bioinformatics* **26**, 139-140 (2010).
53. Yu, G. & He, Q.Y. ReactomePA: an R/Bioconductor package for reactome pathway analysis and visualization. *Mol Biosyst* **12**, 477-479 (2016).
54. G, S.*, et al.* limma: Linear Models for Microarray Data. (2016).
55. Subramanian, A.*, et al.* Gene set enrichment analysis: a knowledge-based approach for interpreting genome-wide expression profiles. *Proc Natl Acad Sci U S A* **102**, 15545-15550 (2005).
56. Maglott, D., Ostell, J., Pruitt, K.D. & Tatusova, T. Entrez Gene: gene-centered information at NCBI. *Nucleic acids research* **39**, D52-57 (2011).

642 57. Leek, J.T., Johnson, W.E., Parker, H.S., Jaffe, A.E. & Storey, J.D. The sva
643 package for removing batch effects and other unwanted variation in high-
644 throughput experiments. *Bioinformatics* **28**, 882-883 (2012).
645 58. Gentleman, R.C.*, et al.* Bioconductor: open software development for
646 computational biology and bioinformatics. *Genome Biol* **5**, R80 (2004).
647 59. Patel, O.*, et al.* Recognition of vitamin B metabolites by mucosal-associated
648 invariant T cells. *Nature communications* **4**, 2142 (2013).

649

650

Acknowledgments

This work was funded by grants to T.S.C.H. from the Wellcome Trust (104553/z/14/z, 211050/Z/18/z). The research was supported by the National Institute for Health Research (NIHR) Oxford Biomedical Research Centre (BRC). The views expressed are those of the authors and not necessarily those of the NHS, the NIHR or the Department of Health. The work was also supported by the National Health and Medical Research Council of Australia (NHMRC) Program Grants 1113293, 1071916, 1016629 and 606788, and Project Grant 1120467. A.J.C. is supported by an ARC Future Fellowship. S.B.G.E. is supported by an ARC DECRA Fellowship. P.K. was supported by an NIHR Senior Fellowship, Oxford Martin School (PK) and the Wellcome Trust (WT109965MA). We are grateful to Dr Brendan Russ and Linda Wakim for assistance and suggestions for experimental design; Dr Ama Essilfie, Prof Richard Strugnell, Frances Oppodisam, Jennifer Davies, Prof Roy Robbins-Browne, Prof Kenneth Beagley and Hayley Newton for bacterial strains; Prof David Jackson for Pam2Cys; Dr Jeffrey Mak for MR1 ligands; Dr Vanta Jameson, Mr Josh Kie at the Flow Cytometry Facilities at the Melbourne Brain Centre and the Peter Doherty Institute; and to Kym Pham and Karey Cheong at the Melbourne Translational Genomic Platform.

Author contributions

TSCH, TLP, LK, SBG, BSM, BR, KP, KC performed the experiments**.** TSCH, MO, EM, AK, MJ analysed the data. TSCH, JM, ZC, AC, ST, PK designed the experiments and managed the study. TSCH, MJ, AC, ZC, JM, PK conceived the work and wrote the manuscript which was revised and approved by all authors.

673

674 **Competing Financial Interests**

675 Z.C., J.McC., and A.C. are inventors on patents describing MR1 tetramers and MR1

676 ligands. The other authors declared no conflict of interest.

677

678 **Materials and Correspondence**

679 Correspondence and material requests should be addressed to TSC Hinks

680 (timothy.hinks@ndm.ox.ac.uk).

681
682

Figures

Figure 1. Costimulatory requirements for MAIT cell activation *in vivo*

(**A**) Representative flow-cytometry plots showing MAIT cell percentage among TCRβ$^+$ lymphocytes in the lungs of C57BL/6 mice with or without prior stimulation with intranasal CpG and 5-OP-RU. Relative (**B**) and absolute (**C**) numbers of MR1-5-OP-RU tetramer$^+$ MAIT cells in the lungs of C57BL/6 mice 7 days after intranasal exposure to specific TLR agonists either alone, or in combination with 76 pmol 6-FP, or with 76 pmol 5-OP-RU. Control mice received nothing (n=4, naïve) or CpG with 5-OP-RU (n=3). Experiments used n=5 (5-OP-RU treated), n=3 (6-FP treated) or n=2 (TLR agonist alone) mice per group. The experiment was subsequently repeated with similar results. Statistical tests: unpaired t tests, comparing TLR + 5-OP-RU with naïve control (n=4), on untransformed (B) or log-transformed (C) data, with Bonferroni corrections * $P<0.05$, *** $P<0.001$.

Figure 2. Reactome pathway analysis of activated MAIT cells

Pathway analysis of human and murine activated MAIT cell transcriptomes. Human peripheral blood 5-OP-RU-stimulated MR1-5-OP-RU-tetramer$^+$ MAIT cells compared with (**A**) naïve CD8$^+$CD45RA$^+$ cells or (**B**) unstimulated MAIT cells. Murine pulmonary MR1-5-OP-RU-tetramer$^+$ MAIT cells day 7 post-infection with *Legionella* were compared with (**C**) naïve CD8$^+$CD44$^-$CD62L$^+$ T cells from uninfected mice or (**D**) MR1-tetramer$^+$ MAIT cells from mice 12 weeks post infection with *Legionella*. Plots show the extent to which named pathways from the curated Reactome database are upregulated. Colour

intensity represents statistical significance of the upregulation, dot size represents the number of genes upregulated in the pathway, x axis represents the proportion of all differentially expressed genes included in the pathway ('gene ratio'). Pathways were selected using a significance threshold of a log fold change > 2 and P <0.01.

Figure 3. Comparison of murine MAIT cell transcriptomes with other cells in Immunological Genome Project dataset

Hierarchical clustering was used to compare transcriptomes of murine pulmonary MAIT cells or naïve $CD8^{+}CD44^{-}CD62L^{+}$ cells with eighty-eight other cell types deposited in the Immunological Genome Project (ImmGen) database. Figure shows a dendrogram (left), ImmGen identifiers (middle) and the full name of each cell type (right). ImmGen samples are identified in white lettering. Samples from the current study are identified in black lettering, with extended lozenges. Cell types are colour-coded: invariant natural killer T cells (iNKT, orange), natural killer (NK) cells (brown), γδ T cells (light green), innate lymphoid cells (ILC, dark green), conventional CD8 T cells (blue), MAIT cells (purple). CD, clonal designation; NCR, NK cell receptor; Teff, effector T cell; Tmem, memory T cell.

Figure 4. Gene set enrichment analysis for tissue repair gene signature in human and murine MAIT cells

Gene set enrichment analysis (GSEA) was used to determine potential enrichment of a tissue repair signature[21] in gene expression profiles from human (A,B) and murine (C,D) MAIT cells. (**A**) GSEA summary plots for 5-OP-RU-stimulated human peripheral blood MAIT cells compared with unstimulated MAIT cells. The gene set is highly enriched:

727 enrichment score (ES) = 0.62, normalised enrichment score (NES) = 1.38, nominal p value
728 <0.01, family-wise error rate (FWER) p value <0.01. (**B**) Heat map of expression of leading
729 edge subset genes within the gene set (red, highest expression, blue, lowest). (**C**) GSEA
730 summary plots for murine pulmonary MAIT cells 7 days post i.n. *L. longbeachae* infection,
731 compared with MAIT cells 12 weeks post infection. The gene set is highly enriched:
732 enrichment score (ES) = 0.85, normalised enrichment score (NES) = 1.23, nominal p value
733 <0.01, family-wise error rate (FWER) p value <0.01. (**D**) Heat map of expression of leading
734 edge subset genes within the gene set (red, highest expression, blue, lowest).

735 **Supplementary figure S1. Tissue distribution of MAIT cells during**
736 **infection *in vivo***

737 Relative frequencies of MR1-5-OP-RU tetramer$^+$ MAIT cells as a proportion of total live
738 TCRβ$^+$ T cells in the peripheral blood, mesenteric lymph node (L.N.), spleen, liver and
739 lungs of C57BL/6 mice before, or after intranasal infection with 1x10^4 CFU *L.*
740 *longbeachae*. Mice were sacrificed before ('uninfected'), or 7 days after infection ('acute'),
741 or at least 12 weeks post infection ('resolution') or 7 days after a second intranasal infection
742 with 2x104 CFU *L. longbeachae* in mice which had recovered from infection 12 weeks
743 previously ('reinfection'). Graph shows combined data from experiments using 3-5 mice
744 per group and performed one-three times.

Supplementary figure S2. Cytometric validation of key differentially expressed genes (human)

(**A**) Representative flow-cytometry plots showing surface expression of the chemokine receptors CCR5, CCR7, CCR2, CCR1, CXCR6, CXCR4, CCR6, CXCR3, and intracellular expression of the cytokines IL-10, IL-17F and LIF. Histograms compare staining of $CD8^+CD45RA^+$ cells (black, dotted) with unstimulated MAIT cells (blue) or MAIT cells after 6 h stimulation with 10 nM 5-OP-RU (red). (**B**) Representative flow-cytometry plots showing expression of the cytokines IL-17A, GM-CSF, IFN-γ and IL-10, by intracellular cytokine staining. Histograms compare staining of MR1-5-OP-RU $tetramer^+$ MAIT cells after 6 h stimulation with 10 nM 5-OP-RU in the presence of brefeldin A (right) with unstimulated cells (middle) and tetramer-negative, $CD8^+CD45RA^+$ naïve T cells (left). Figures in brackets represent percentage of MAIT cells (top / middle) or of $CD8^+CD45RA^+$ T cells (bottom) expressing the cytokine. Results are representative of three independent donors.

Supplementary figure S3. Cytometric validation of key differentially expressed genes (murine)

Representative flow-cytometry plots showing expression of the cytokines IL-17A, TNF, IL-10, TRANCE (TNFSF11), GM-CSF, IL-17F and GITRL (TNFSF18) by intracellular cytokine staining on murine pulmonary T cells. Histograms compare staining of $CD44^-$ $CD62L^+$ T cells from uninfected mice (left) with MR1-5-OP-RU $tetramer^+$ MAIT cells either 7 days ('acute', middle left) or 12 weeks ('resolution', middle right) after infection with 1 $x10^4$ CFU intranasal *L. longbeachae,* or 7 days after reinfection with 2 $x10^4$ CFU

i.n. *L. longbeachae* in mice previously infected 12 weeks prior with 10^4 CFU i.n. *L. longbeachae* ('reinfection', right). Cells were incubated for 4 h in the presence of brefeldin A without (A, *ex vivo*) or with (B, stimulated) PMA and ionomycin. Figures in brackets represent percentage of $CD44^-CD62L^+$ T cells (left, lower quadrants) or MR1-tetramer$^+$ MAIT cells (middle and right, upper quadrants), or MR1-tetramer$^-$ conventional T cells (middle and right, lower quadrants) expressing the cytokine. Results are representative of three independent replicates performed on two separate days.

Supplementary figure S4. Cytometric gating strategy (human)

Human peripheral blood lymphocytes were identified, and doublets excluded, using forward and side scatter characteristics. Dead cells were excluded using Zombie Yellow viability stain, then populations were gated on $CD3^+$ cells, then on either MR1-5-OP-RU tetramer conjugated to PE or BV421 for MAIT cells, or on CD8 and CD45RA to identify naïve $CD8^+CD45RA^+$ cells. Histograms compare staining of $CD8^+CD45RA^+$ cells (black) with unstimulated MAIT cells (blue) or MAIT cells after 6 h stimulation with 10 nM 5-OP-RU (red). For intracellular cytokines, where basal cytokine secretion was minimal, gates were set on the unstimulated MAIT cell sample.

Supplementary figure S5. Cytometric gating strategy (murine)

Pulmonary lymphocytes were identified, and doublets excluded, using forward and side scatter characteristics. Dead cells were excluded using Zombie Yellow viability stain, then populations were gated on $CD19^-CD45.2^+$ cells, then TCRβ+ cells and finally MR1-5-OP-RU tetramer$^+$ MAIT cells, or $CD44^-CD62L^+$ T cells.

Tables

Table 1. Definitions of transcriptomic samples

Species	Condition	Cell type	Cytometric definition	Samples (n)
Human	Unstimulated	Naïve cytotoxic T cell	Live CD3+CD8+45RA+	3
Human	Unstimulated	MAIT cell	Live $CD3^{+}$TCR-Vα7.2^{+}MR1-5OP-RU-$tetramer^{+}$	3
Human	Stimulated (5-OP-RU)	MAIT cell	Live $CD3^{+}$TCR-Vα7.2^{+}MR1-5OP-RU-$tetramer^{+}$	3
Murine	Uninfected	Naïve cytotoxic T cell	Live $CD3^{+}45.2^{+}19^{-}TCR\beta^{+}44^{-}62L^{+}$	3
Murine	Acute infection (7 days post infection)	MAIT cell	Live $CD3^{+}45.2^{+}19^{-}TCR\beta^{+}$MR1-5-OP-RU-$tetramer^{+}$	3
Murine	Resolution (12 w post infection)	MAIT cell	Live $CD3^{+}45.2^{+}19^{-}TCR\beta^{+}$MR1-5-OP-RU-$tetramer^{+}$	3
Murine	Reinfection (7 days post reinfection)	MAIT cell	Live $CD3^{+}45.2^{+}19^{-}TCR\beta^{+}$MR1-5-OP-RU-$tetramer^{+}$	3

Three biological replicates of each sample typed were submitted for analysis.

Table 2. Numbers of differentially expressed genes

	Human			Murine		
	Unstimulated MAIT v Unstimulated CD8+45RA+	Stimulated MAIT v Unstimulated MAIT	Stimulated MAIT v Unstimulated CD8+45RA+	Acute infection MAIT v Uninfected $CD8^{+}44^{Lo}62^{Hi}$	Resolved infection MAIT v Acute infection MAIT	Reinfection MAIT v Acute infection MAIT
Number of upregulated genes	411	1384	1651	1985	942	235
Number of downregulated genes	557	1843	2512	1773	947	241

Genes shown are censored at FDR P ≤0.05 and log(2) fold change of ±1.

796 **Table 3.** Differentially expressed cytokine genes. Human.
797

Stimulated MAIT v Unstimulated CD8+45RA+					
Gene	**Log fold change**	**Log CPM**	**LR**	***P* value**	**FDR *P* value**
CSF2	15	7.4	62	3E-15	0.00
IL17A	12	4.9	74	8E-18	0.00
IL2	11	4.0	42	1E-10	0.00
LIF	8.9	1.8	26	3E-07	0.00
TNF	8.7	9.0	59	2E-14	0.00
IFNG	8.4	8.4	51	1E-12	0.00
IL17F	8.3	1.2	32	1E-08	0.00
TNFSF14	5.3	8.0	113	2E-26	0.00
CSF1	5.2	5.1	120	7E-28	0.00
IL26	4.6	1.8	16	7E-05	0.00
LTA	3.3	7.0	48	4E-12	0.00
TGFA	2.9	3.3	19	1E-05	0.00
TNFSF13B	2.6	3.2	12	0.0004	0.00

Stimulated MAIT v Unstimulated MAIT					
Gene	**Log fold change**	**Log CPM**	**LR**	***P* value**	**FDR *P* value**
CSF2	15	7.4	64	1E-15	0.00
IL17A	12	4.9	77	1E-18	0.00
IFNG	9.7	8.4	61	6E-15	0.00
IL17F	8.3	1.2	35	3E-09	0.00
IL2	8.0	4.0	33	1E-08	0.00
TNF	6.3	9.0	38	8E-10	0.00
LIF	4.2	1.8	12	0.0005	0.00
IL10	4.1	1.5	14	0.0002	0.00
TNFSF14	3.2	8.0	52	6E-13	0.00
CSF1	3.2	5.1	59	2E-14	0.00
LTA	3.1	7.0	43	7E-11	0.00
IL16	-1.1	9.3	5.6	0.018	0.04
TGFA	-1.6	3.3	7.4	0.006	0.02

Unstimulated MAIT v Unstimulated CD8+45RA+					
Gene	**Log fold change**	**Log CPM**	**LR**	***P* value**	**FDR *P* value**
LIF	4.7	1.8	7.2	0.007	0.02
TGFA	4.4	3.3	43	6E-11	0.00
TNF	2.4	9.0	7.9	0.005	0.02
TNFSF13B	2.3	3.3	9.5	0.002	0.01
TNFSF14	2.1	8.0	22	2E-06	0.00
CSF1	2.0	5.1	21	7E-06	0.00
IL15	1.9	2.3	5.8	0.02	0.04
IL24	-1.8	2.4	6.2	0.01	0.04
CXCR2	-4.0	3.0	9.7	0.001	0.01
CXCR1	-4.1	2.6	14	0.0001	0.00

IL23A	2.3	4.7	12	0.0004	0.00
IL32	-1.2	9.7	12	0.0005	0.00
IL16	-1.5	9.3	11	0.001	0.00
IL24	-2.0	2.4	7.7	0.005	0.01
IL18BP	-3.6	5.1	57	6E-14	0.00
CXCR2	-4.9	3.0	13	0.0002	0.00
CXCR1	-9.8	2.6	37	1E-09	0.00

IL32	-1.6	9.7	20	8.1E-06	0.00
IL18BP	-3.0	5.1	40	2.9E-10	0.00
CXCR1	-5.7	2.6	13	0.0004	0.00

Genes shown are censored at FDR P ≤0.05 and log(2) fold change of ±1,and ordered by log fold change. Genes highlighted in bold are differentially expressed in both human and mouse. CPM, Counts per million; FDR, false discovery rate; LR, likelihood ratio.

Table 4. Differentially expressed cytokine genes. Mouse.

Acute infection MAIT v Uninfected $CD8^{+}44^{Lo}62^{Hi}$						Resolved infection MAIT cells v Acute infection MAIT cells					
Gene	**Log fold change**	**Log CPM**	**LR**	***P* value**	**FDR *P* value**	**Gene**	**Log fold change**	**Log CPM**	**LR**	***P* value**	**FDR *P* value**
Il17a	14	7.3	316	9E-71	1E-68	Tnfsf18 (GITRL)	5.9	-0.52	14	0.0002	0.001
Ifng	12	5.9	222	3E-50	2E-48	Tnfsf11 (TRANCE)	3.2	6.6	67	3E-16	4E-14
Csf2	11	4.8	208	4E-47	3E-45	Il15	1.9	0.88	6.7	0.0096	0.03
Il17f	11	4.9	171	5E-39	2E-37	Tgfb3	1.4	4.0	16	6E-05	0.0005
Lif	10	3.6	132	1E-30	5E-29	Il6st	1.3	6.7	9.9	0.002	0.008
Il22	9.1	2.4	43	4E-11	4E-10	Il17f	1.1	4.9	8.5	0.004	0.02
Il21	7.5	0.65	23	2-06	1E-05	Il21	-3.8	0.65	11	0.0008	0.005
Tnf	4.5	6.0	188	1E-42	6E-41	Il17a	-2.4	7.3	38	9E-10	38E-08
Lta (TNFb / lymphotoxin A)	3.8	6.2	110	9E-26	3E-24	Ifng	-2.4	5.9	35	3E-09	8E-08
Il1b	2.6	4.5	6.2	0.01	0.03	Tnfsf10 (TRAIL)	-1.6	4.0	19	2E-05	0.0002
Tnfsf11 (TRANCE)	2.3	6.6	35	3E-09	2E-08	Lif	-1.4	3.6	11	0.0009	0.005
Csf1 (M-CSF)	2.3	3.0	11	0.0009	0.003						
Tnfsf10 (TRAIL)	1.1	4.0	9.7	0.002	0.005						

Reinfection MAIT cells v Acute infection MAIT cells					
Gene	**Log fold change**	**Log CPM**	**LR**	***P* value**	**FDR *P* value**
Csf1 (M-CSF)	2.2	3.0	12	0.0006	0.01
Il6st	1.5	6.7	14	0.0002	0.005
Tnfsf11 (TRANCE)	1.3	6.6	14	0.0002	0.007
Il17a	-1.5	7.3	15	9.7E-05	0.003
Csf2 (GM-CSF)	-1.2	4.8	12	0.0006	0.01

Genes shown are censored at FDR P ≤0.05 and log(2) fold change of ±1, and ordered by log fold change. Genes highlighted in bold are differentially expressed in both human and mouse. CPM, Counts per million; FDR, false discovery rate; LR, likelihood ratio.

Table 5. Gene set enrichment analysis for Tissue Repair set.

Human Stimulated MAIT v Unstimulated MAIT				
Gene	**Rank in gene list**	**Rank metric score**	**Running Enrichment score**	**Core enrichment**
CCL3	16	7.566	0.180	Yes
TNF	63	4.421	0.282	Yes
CSF2	85	4.012	0.376	Yes
VEGFA	87	3.990	0.471	Yes
CSF1	105	3.700	0.559	Yes
THBS1	226	2.790	0.614	Yes
HIF1A	594	1.725	0.618	Yes
FURIN	1763	0.836	0.522	No
VEGFB	2560	0.539	0.456	No
MMP28	3207	0.339	0.399	No
HMGB1	5005	-0.120	0.223	No
PTGES2	5279	-0.189	0.200	No
PDGFB	5399	-0.218	0.194	No
TGFB1	5973	-0.374	0.146	No
DISP1	6691	-0.589	0.088	No
TGFA	9539	-2.469	-0.136	No
MMP25	9697	-2.794	-0.085	No
WNT1	10012	-4.987	0.003	No

Murine Acute infection v Resolved infection				
Gene	**Rank in gene list**	**Rank metric score**	**Running Enrichment score**	**Core enrichment**
HBEGF	5	12.242	0.162	Yes
CSF2	33	11.994	0.319	Yes
MMP25	97	7.929	0.417	Yes
CXCL10	210	5.741	0.481	Yes
AREG	216	5.579	0.555	Yes
JAG1	234	5.371	0.625	Yes
TNF	311	4.744	0.679	Yes
PDGFB	375	4.226	0.729	Yes
TGFB3	414	3.921	0.777	Yes
CXCL2	529	3.295	0.808	Yes
FURIN	721	2.474	0.820	Yes
IL1B	772	2.296	0.845	Yes
TGFB1	1134	1.427	0.824	No
HIF1A	1464	1.033	0.802	No
THBS1	1761	0.801	0.780	No
VEGFB	2604	0.398	0.692	No
HMGB1	3518	0.118	0.594	No
PTGES2	4382	-0.084	0.500	No

DISP1	8193	-1.502	0.101	No

Genes set enrichment analysis (GSEA) was used to determine potential enrichment of a tissue repair signature[21] in gene expression profiles of 5-OP-RU-stimulated human peripheral blood MAIT cells compared with unstimulated MAIT cells (left) and of murine pulmonary MAIT cells 7 days post i.n. *L. longbeachae* infection, compared with MAIT cells 12 weeks post infection (right). Genes are ordered by their position in the list of genes ranked by their normalised enrichment score (ES). Genes highlighted in bold are also significant in the equivalent analysis for murine MAIT cells. Running enrichment score: ES at this point in the ranked list of genes. Core enrichment genes contribute to the leading-edge subset of genes that contribute most to the enrichment result.

Supplementary table S1. Toll like receptor agonists used in murine experiments

Supplementary table S2. Comprehensive list of differentially expressed genes. Human.

Genes shown are censored at FDR P ≤0.05 and log(2) fold change of ±1, and ordered by log fold change. CPM, Counts per million; FDR, false discovery rate; LR, likelihood ratio.

Supplementary table S3. Comprehensive list of differentially expressed genes. Murine.

Genes shown are censored at FDR P ≤0.05 and log(2) fold change of ±1, and ordered by log fold change. CPM, Counts per million; FDR, false discovery rate; LR, likelihood ratio.

Supplementary table S4. TCR usage overrepresented genes. Human.

Genes shown are censored at FDR P ≤0.05 and log(2) fold change of ±1, and ordered by log fold change. CPM, Counts per million; FDR, false discovery rate; LR, likelihood ratio.

Supplementary table S5. TCR usage overrepresented genes. Murine.

Genes shown are censored at FDR P ≤0.05 and log(2) fold change of ±1, and ordered by log fold change. CPM, Counts per million; FDR, false discovery rate; LR, likelihood ratio.

Supplementary table S6. Differentially expressed cytokine receptors. Human.

Genes associated with formation of T cell memory which are found to be differentially expressed in this dataset. Genes shown are censored at FDR P ≤0.05 and ordered by log fold change. CPM, Counts per million; FDR, false discovery rate; LR, likelihood ratio.

Supplementary table S7. Differentially expressed cytokine receptors. Murine.

Genes shown are censored at FDR P ≤0.05 and log(2) fold change of ±1, and ordered by log fold change. CPM, Counts per million; FDR, false discovery rate; LR, likelihood ratio.

Supplementary table S8. Differentially expressed surface markers (Cluster of Differentiation molecules). Human

Genes shown are censored at FDR P ≤0.05 and log(2) fold change of ±1, and ordered by log fold change. CPM, Counts per million; FDR, false discovery rate; LR, likelihood ratio.

Supplementary table S9. Differentially expressed surface markers (Cluster of Differentiation molecules). Murine.

Genes shown are censored at FDR P ≤0.05 and log(2) fold change of ±1, and ordered by log fold change. CPM, Counts per million; FDR, false discovery rate; LR, likelihood ratio.

Supplementary table S10. Differentially expressed chemokines. Human.

Genes shown are censored at FDR P ≤0.05 and log(2) fold change of ±1, and ordered by log fold change. Genes highlighted in bold are also significant in the equivalent analysis for murine MAIT cells. CPM, Counts per million; FDR, false discovery rate; LR, likelihood ratio.

Supplementary table S11. Differentially expressed chemokines. Murine.

Genes shown are censored at FDR P ≤0.05 and log(2) fold change of ±1, and ordered by log fold change. Genes highlighted in bold are also significant in the equivalent analysis for human MAIT cells. CPM, Counts per million; FDR, false discovery rate; LR, likelihood ratio.

865 **Supplementary table S12. Differentially expressed chemokine receptors.**

866 **Human.**

867 Genes shown are censored at FDR P ≤0.05 and log(2) fold change of ±1, and ordered by
868 log fold change. Genes highlighted in bold are also significant in the equivalent analysis
869 for murine MAIT cells. CPM, Counts per million; FDR, false discovery rate; LR,
870 likelihood ratio.

871 **Supplementary table S13. Differentially expressed chemokine receptors.**

872 **Murine.**

873 Genes shown are censored at FDR P ≤0.05 and log(2) fold change of ±1, and ordered by
874 log fold change. Genes highlighted in bold are also significant in the equivalent analysis
875 for human MAIT cells. CPM, Counts per million; FDR, false discovery rate; LR, likelihood
876 ratio.

877 **Supplementary table S14. Tissue repair gene signature.**

878 Murine tissue repair signature gene set from Linehan *et al*[21] used in both murine and human
879 GSEA analyses.

880 **Supplementary table S15. Cytometry antibodies.**

881

882 Figure 1

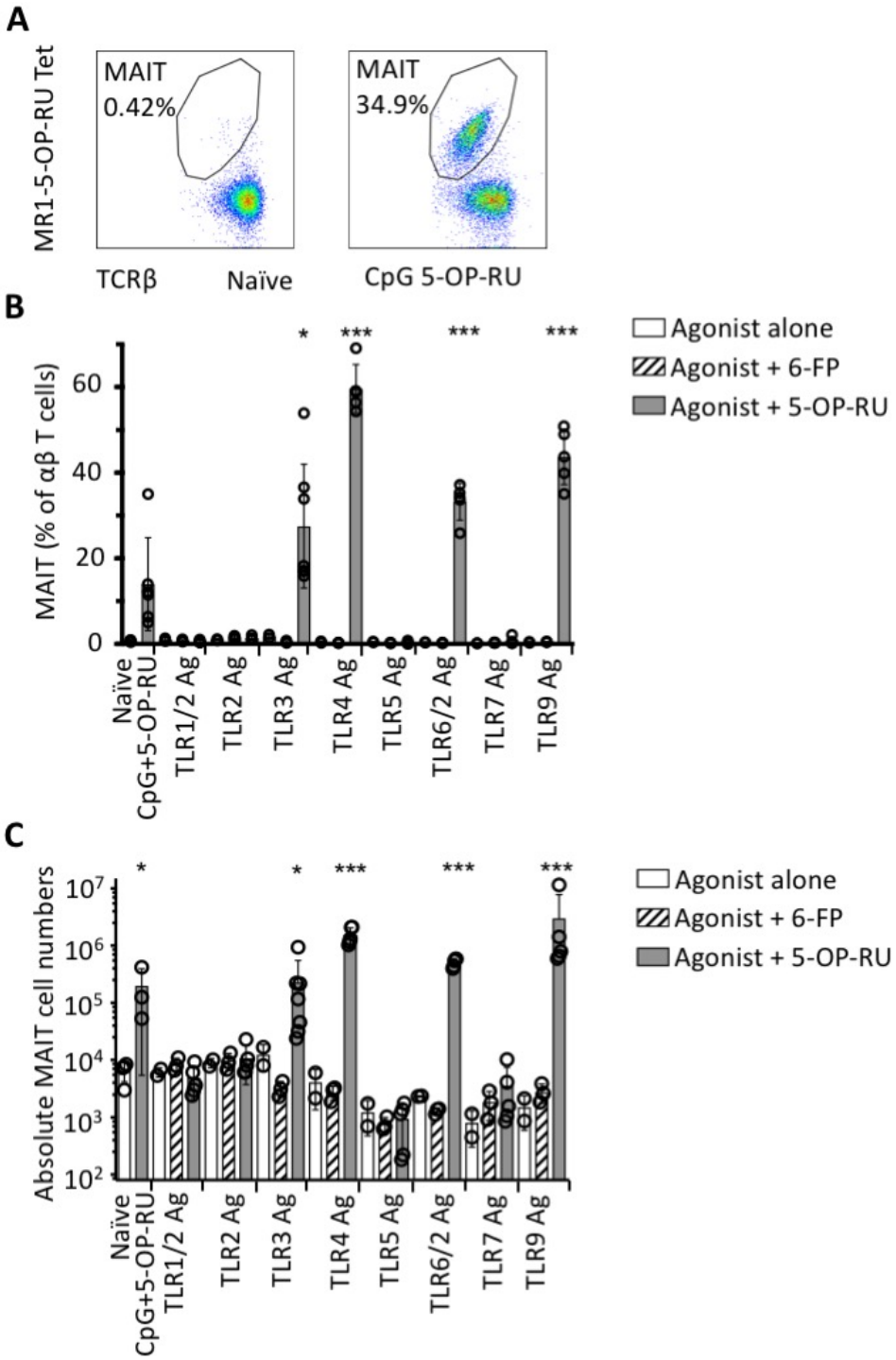

883

884 Figure 2

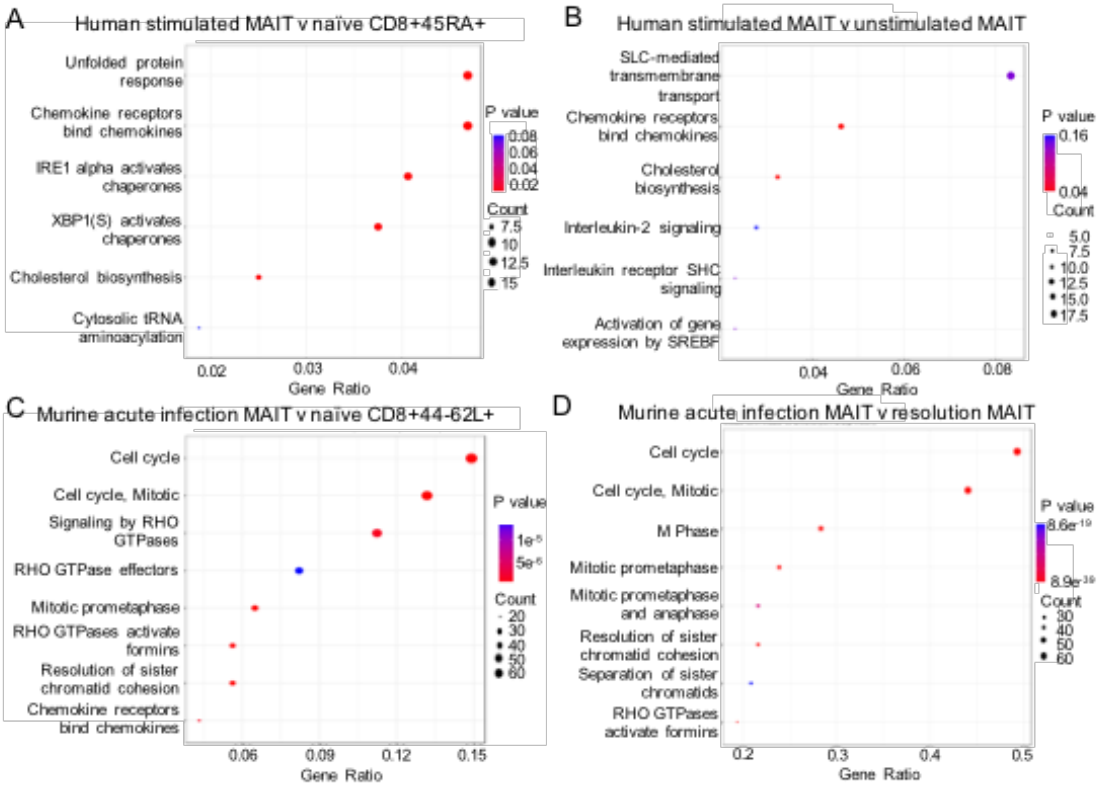

885
886

887 Figure 3

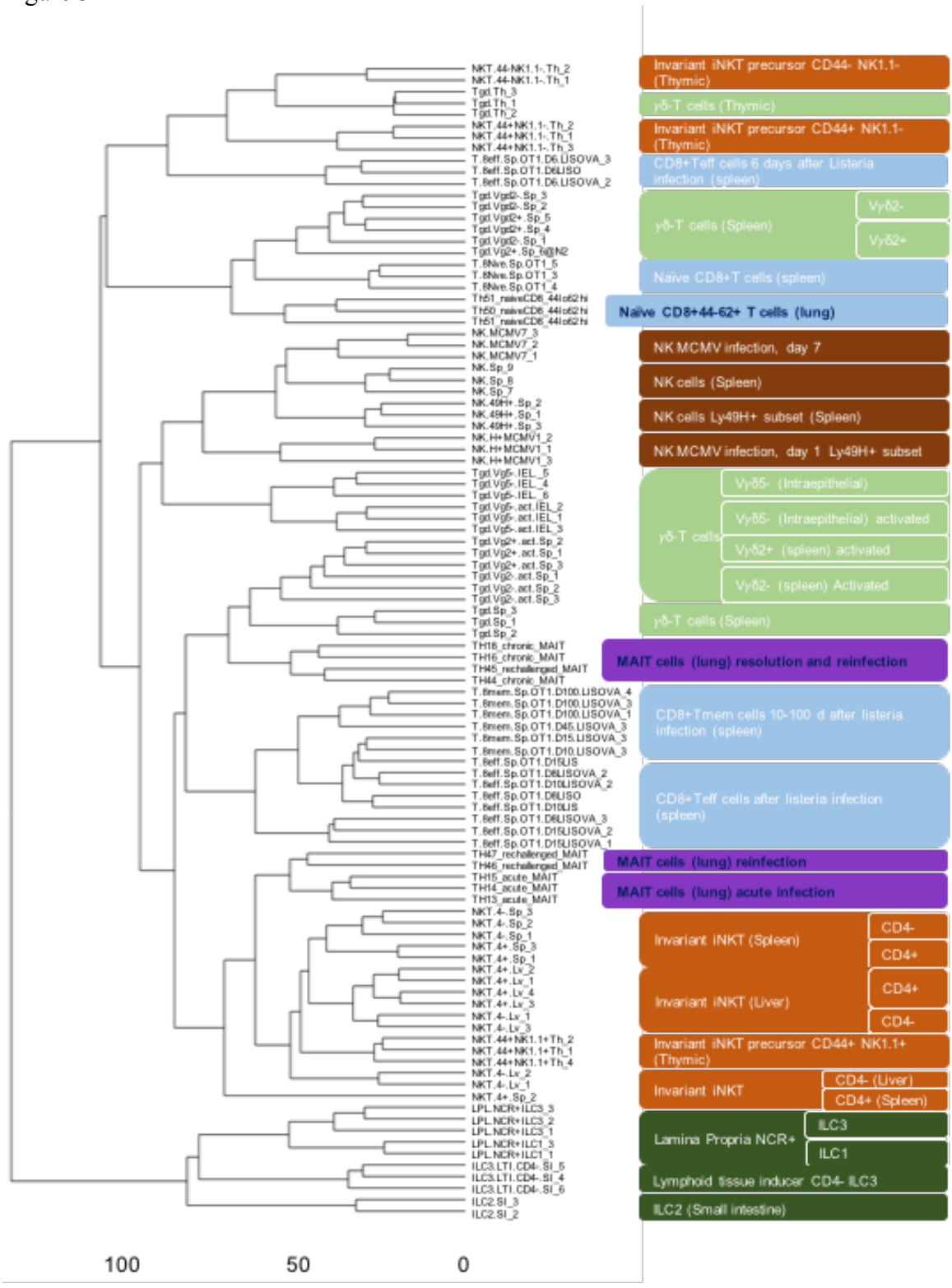

888
889

890 Figure 4

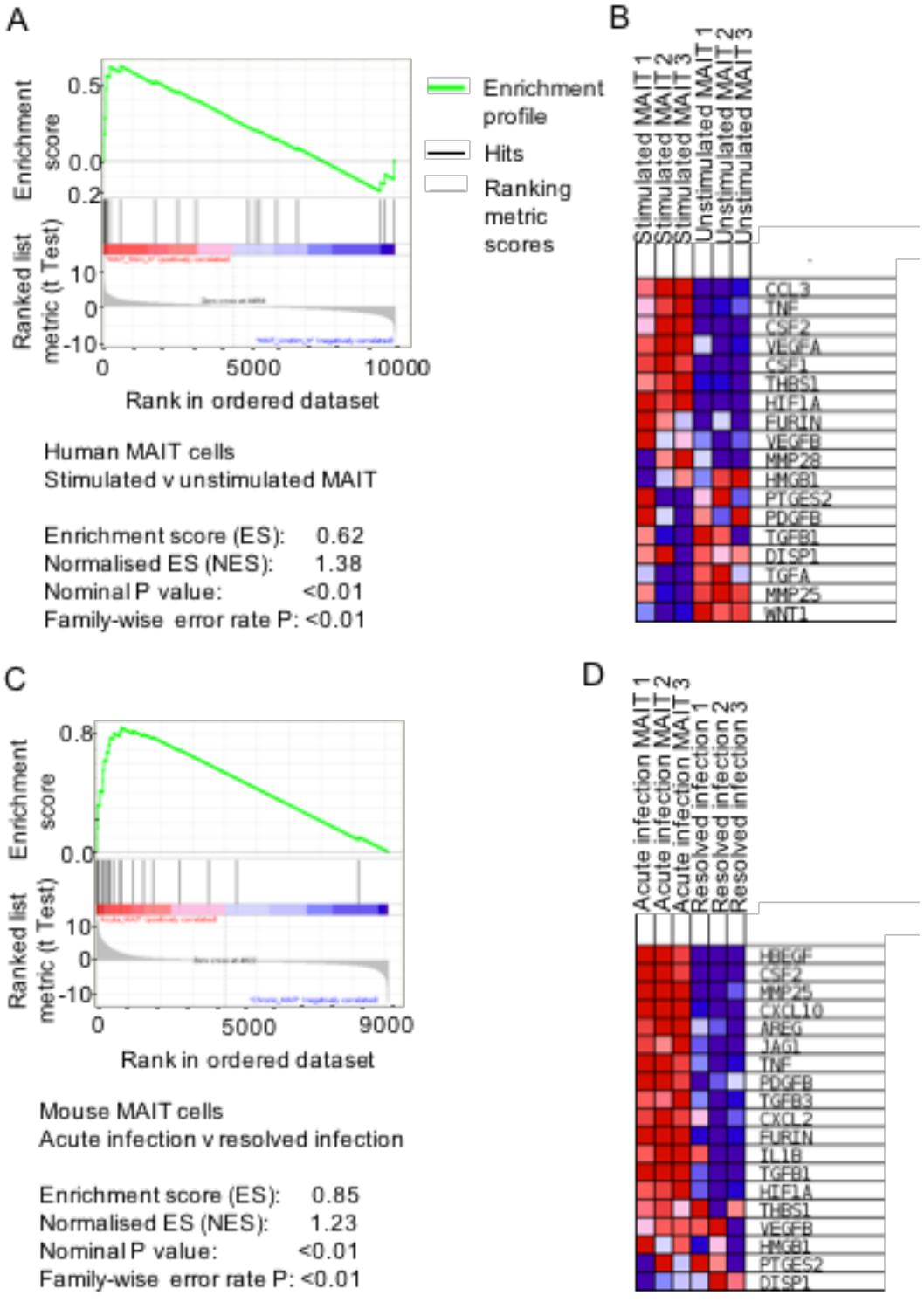

891
892

893 Supplementary figure S1

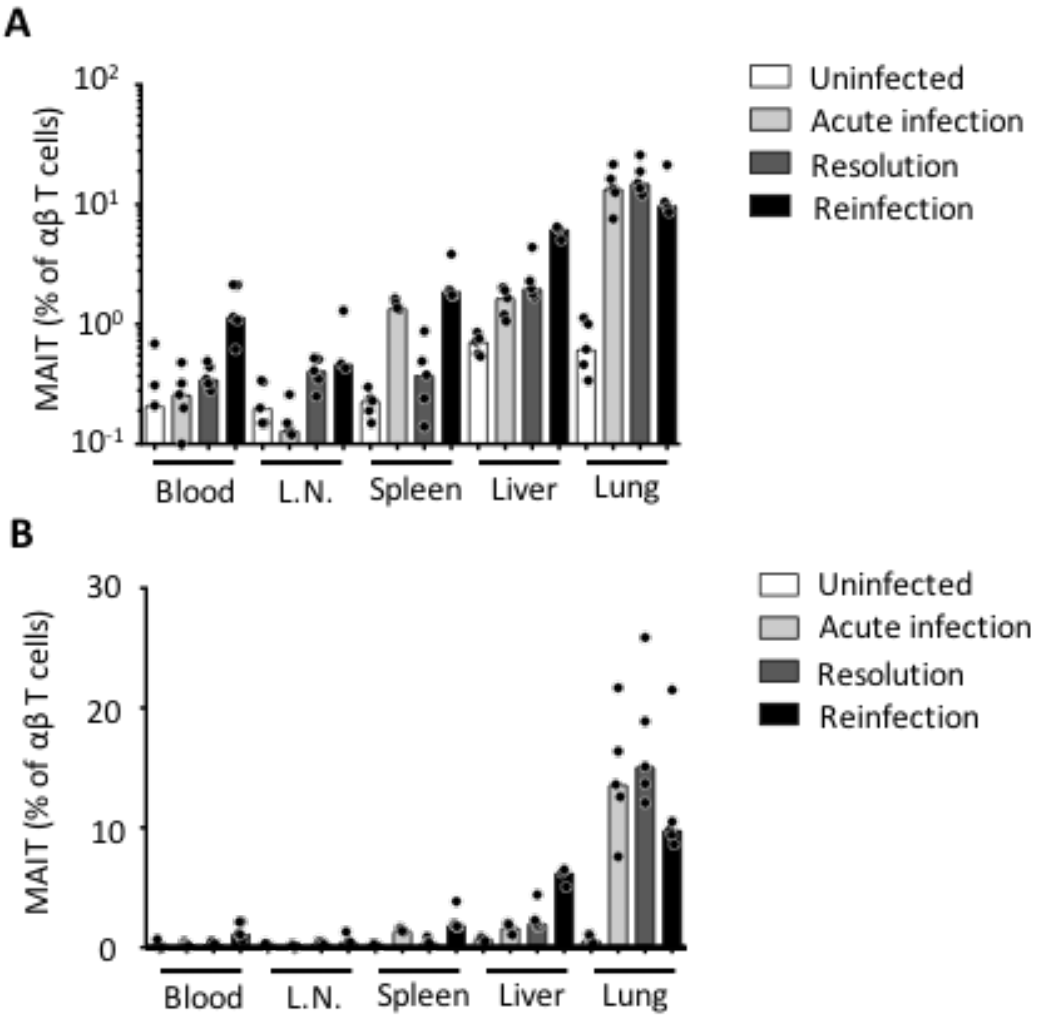

894

895

896

897 Supplementary figure S2

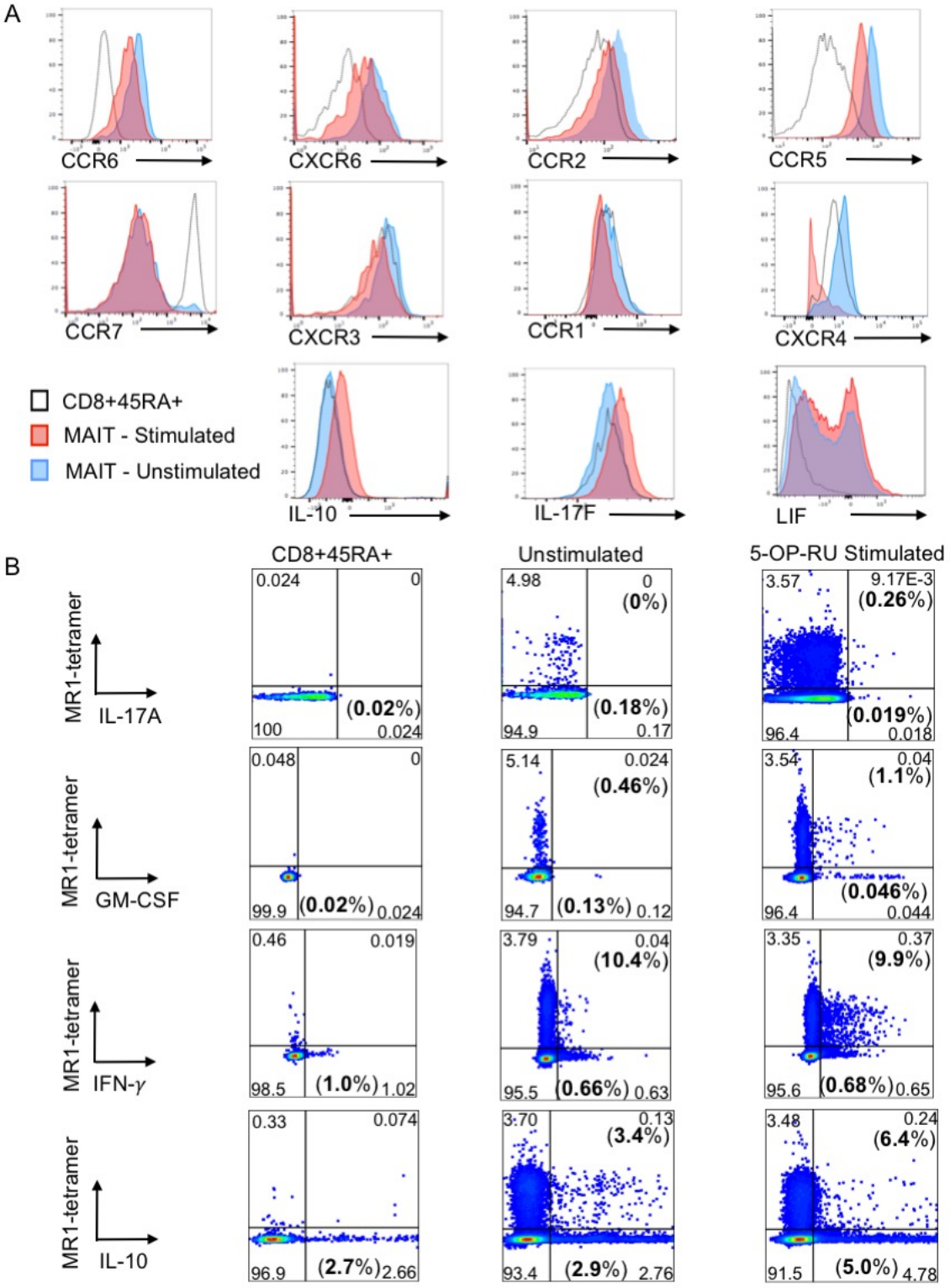

898
899

900 Supplementary figure S3

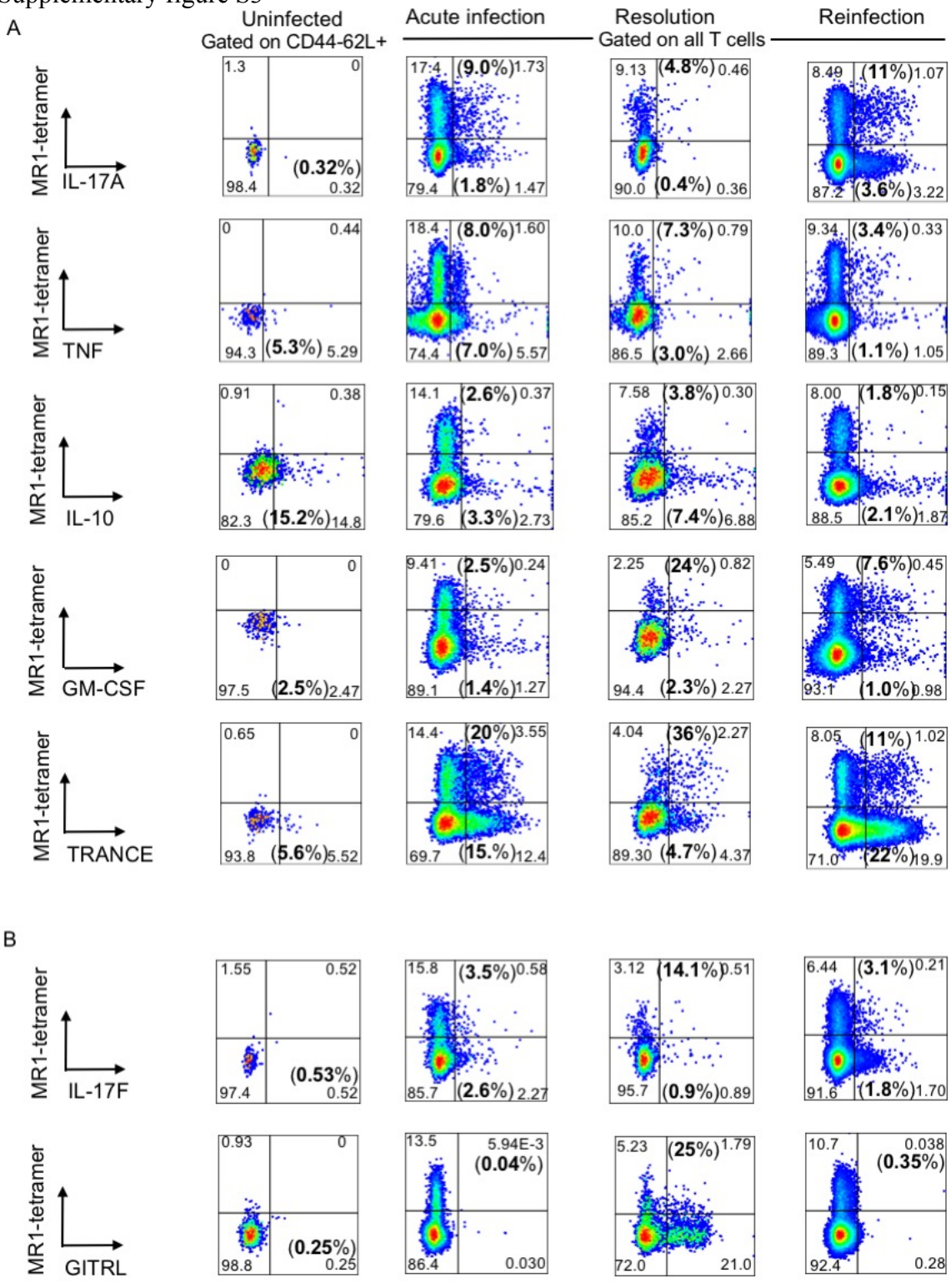

901
902

903 Supplementary figure S4
904

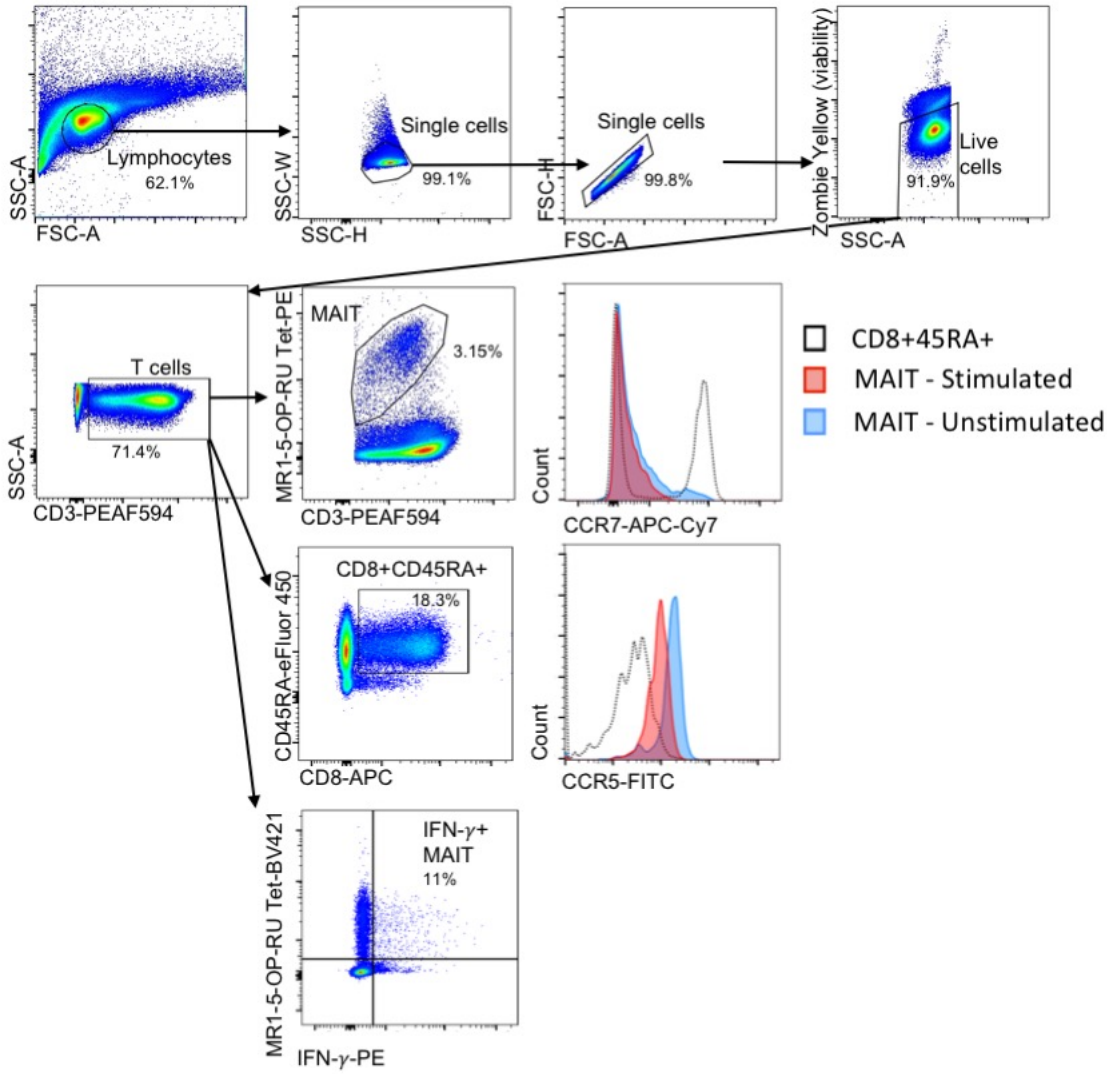

905

906 Supplementary figure S5

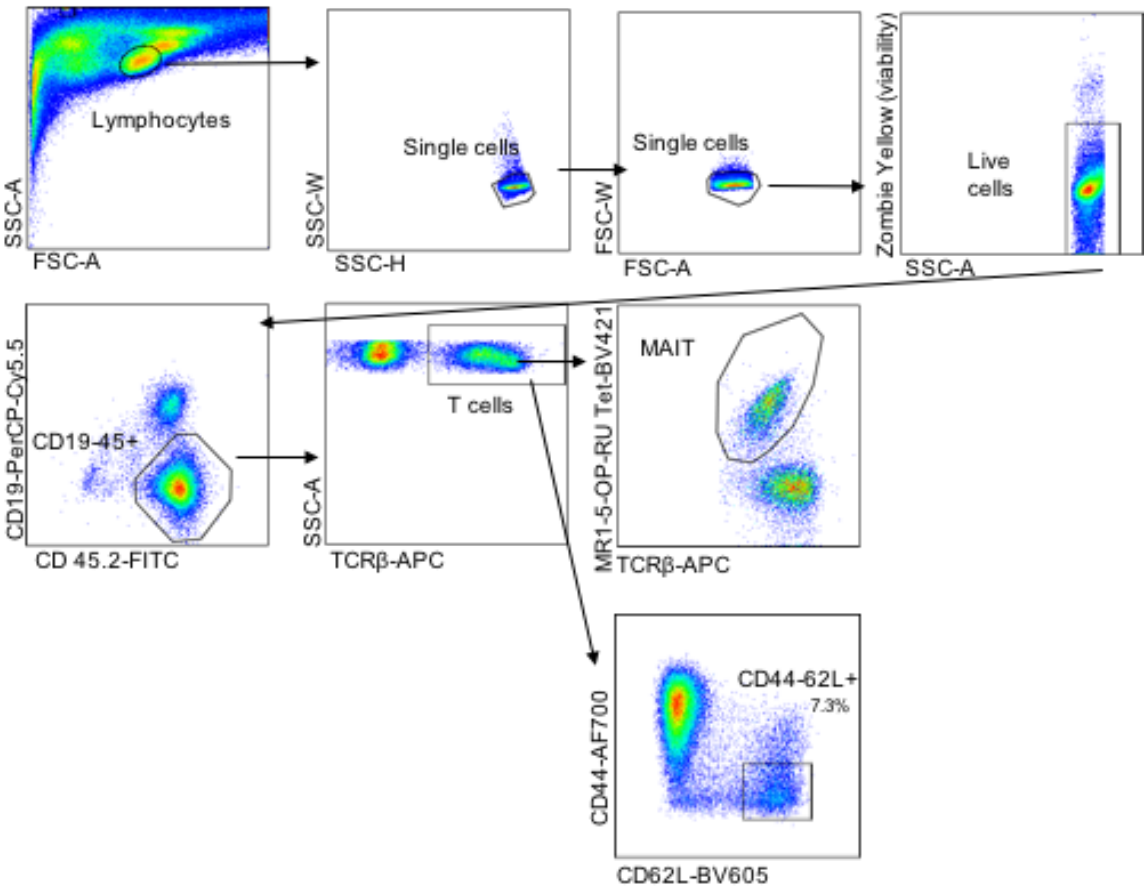

907